ABSTRACT

Title of Thesis:	ROTOR SHAPE MANIPULATION FOR THE DESIGN OF AN ALTERNATOR-BASED REGNERATIVE BRAKING SYSTEM
	Brendan Bradley, Clifton Buxbaum, Dain Golsen, Sean Haliyur, Nikhil Hosamane, Alan Kaplan, Avery Layne, Trisha Patel, Alexander Piqué, Zachary Rodriguez, Zachary Spawn, Bryan Zeug
Thesis Directed By:	Bryan Quinn, Department of Electrical and Computer Engineering

To widen the scope of hybrid technology, Team DRIVE studied the implementation of an alternator-based regenerative braking system onto an automobile's drive shaft. The team hypothesized that salient rotors were more ideal for an alternator-based regenerative braking system than the standard Lundell rotor due to their improved efficiency at lower angular velocities. The team conducted computer simulations and physical experiments to evaluate the performance of three electromagnet rotors: a 4-pole and 8-pole salient rotor, and a Lundell rotor. ANSYS Maxwell was used to optimize the geometry of the salient rotors. A test apparatus was designed to test the Lundell rotor by simulating driving conditions. Recommendations were made for the implementation of a salient rotor in an alternator-based regenerative braking system.

ROTOR SHAPE MANIPULATION FOR THE DESIGN OF AN ALTERNATOR-BASED REGNERATIVE BRAKING SYSTEM

By

Team DRIVE
Brendan Bradley, Clifton Buxbaum, Dain Golsen, Sean Haliyur, Nikhil Hosamane, Alan Kaplan, Avery Layne, Trisha Patel, Alexander Piqué, Zachary Rodriguez, Zachary Spawn, Bryan Zeug
Mentor: Bryan Quinn

Thesis submitted in partial fulfillment of the requirements of the
Gemstone Honors Program,
University of Maryland
2018

Advisory Committee:
Bryan Quinn, Chair
Professor Steven Mark Anlage
Dr. Brian Beaudoin
Professor F. Patrick McCluskey
Dr. Eric Montgomery
Dr. Vincent Nguyen
Aynsley Toews
Nevenka Zdravkovska, Librarian

Acknowledgements

Team DRIVE would like to thank the Gemstone staff for always being available to answer our questions and for accompanying us every step of the way. We would also like to thank Elizabeth Soergel and Nevenka Zdravkovska for providing valuable feedback during our research. We would also like to thank the Spawn Family, the Golsen Family, Michael Strah, and Hongyang Jiang for their generous contributions to our research. Also, we would also like to thank EMWorks for permitting us to use their EMS software for our simulations. We would also like to thank the UMD Sustainability Fund for helping fund our research. Finally, we would like to thank our mentor, Bryan Quinn, for accommodating us in his lab and for always having a positive attitude when the outlook looked rather bleak. Without his help and guidance, we would still be spinning our wheels.

Table of Contents

List of Tables

List of Figures

Chapter 1: Introduction

1.1 Overview

The hybrid car is a vehicle powered by both electricity and fossil fuels. These energy efficient vehicles are pivotal in the alleviation of fossil fuel usage and foreign oil dependency. The transportation sector produces 20.449% of CO_2 emissions, and 90% of the transportation sector related CO_2 emissions is a result of road transportation [1], [2]. However, some consumers continue to avoid hybrid cars due to unattractive stigmas such as the short range of battery, poor acceleration, and lack of aesthetic appeal that come with buying a hybrid [3]. Even though hybrids are an effective way to reduce fossil fuel consumption, and therefore air pollution, the technology cannot reduce global emissions if consumers choose not to buy them. In order to increase the appeal of hybrid vehicles, the image and ubiquity of the vehicles must be improved. This task can be accomplished by redesigning combustion-powered vehicles to create an improved and appealing hybridized vehicle.

Most hybrid cars are limited in terms of model availability and can benefit from an expansion of all-wheel drive (AWD) and rear-wheel drive (RWD) technology [3]. Both AWD and RWD vehicles contain a drive shaft as a crucial part of their powertrain [4] . Considering energy can be harvested and collected from numerous locations on a car, the drive shaft presents an alternative source of recapturing energy. Therefore, Team DRIVE's solution to expanding the scope of hybrid vehicles was to implement an alternator-based regenerative braking system on the drivetrain of RWD and AWD cars, specifically on the drive shaft. This was accomplished using simulations and experiments to predict the electrical power production of Lundell and salient rotor alternators when integrated onto a drive shaft system. The team's recommendations

can be used in further testing simulations that can lead to an eventual system integration for those vehicles. As a result, Team DRIVE will have recommended an improved self-recharging hybrid design in an effort to reduce air pollution and foreign oil dependency.

1.2 Statement of Purpose

The focus of this project is on the wasted energy that is generated from the drive shaft. Current technology for harvesting wasted energy from a vehicle's drive shaft was found to be unsustainable. Because of this, the bulk of the material discussed will pertain to a more novel method of capturing waste energy from a drive shaft, such as the implementation of an alternator that can convert mechanical energy into electrical energy. Throughout the course of the literature review, the team will explain the physics behind the operation of alternators and regenerative braking technology and the importance of expanding the scope of hybrid vehicles.

For feasibility purposes, the team will only evaluate the impact of different alternator rotors on the performance of the alternator-based regenerative braking system. The main variables that will be measured are power output and braking torque of the alternator. Power output is an important variable to measure because it directly correlates to a regenerative braking system's ability to recapture wasted energy. Braking torque is another important variable to measure because it can be used to evaluate a regenerative braking system's ability to act as a supplementary braking system. The team will compare the performance of the standard alternator rotor, which is called the Lundell rotor, and two prototype rotors, a 4 and 8-pole salient rotor, through the use of simulations and experiments.

It is important to consider that since no such device has been implemented in the past, any positive power output and positive braking torque will be registered as a success. The influence of the added weight of the alternator on the overall vehicle fuel efficiency can be considered negligible. In the case of a base model Ford F150, the alternator system adds roughly 10 lbs which amounts to 0.25% of the 4,069 lbs curb weight [5]. Reducing vehicle weight by 10% increases fuel efficiency by 8% and assuming a similar correlation for increases in weight, the alternator system would reduce fuel efficiency by 0.2% [6]. In order to design and test the combinations, Team DRIVE was split into sub-teams to concentrate efforts towards the different tasks. The team created a test rig that simulated the drive shaft of a RWD or AWD vehicle. Alternator prototypes were recommended for the implementation into an alternator-based regenerative braking system for drive shafts. Furthermore, magnetic field simulations were implemented to design possible rotor prototypes. Through testing, the team intended to answer one main question: which alternator rotor will maximize the electrical energy production and braking torque of the alternator-based regenerative braking system for vehicle drive shaft application?

The team will test the hypothesis that - when comparing an 8-pole electromagnetic rotor design, a 4-pole electromagnetic rotor design, and a Lundell rotor design - a greater positive net power output and braking torque will be achieved with the 8-pole rotor. The 8-pole rotor design offers more accuracy in controlling the movement and rotation of the system, in addition to offering a departure from the standard claw-pole type rotor configuration [7].

Chapter 2: Literature Review

2.1 Differences in Drivetrains

In order to justify the implementation of regenerative braking technology, the powertrain technology that utilizes a drive shaft must also be justified. For commercial vehicles that are available to the general public, there are three main types of drivetrain systems: front-wheel drive (FWD), RWD, and AWD. RWD and AWD vehicles feature a drive shaft, a component of the drive train that brings power to the rear of the vehicle, as shown in Fig. 1. FWD vehicles keep the power in the front of the vehicle, thus eliminating the need for a drive shaft.

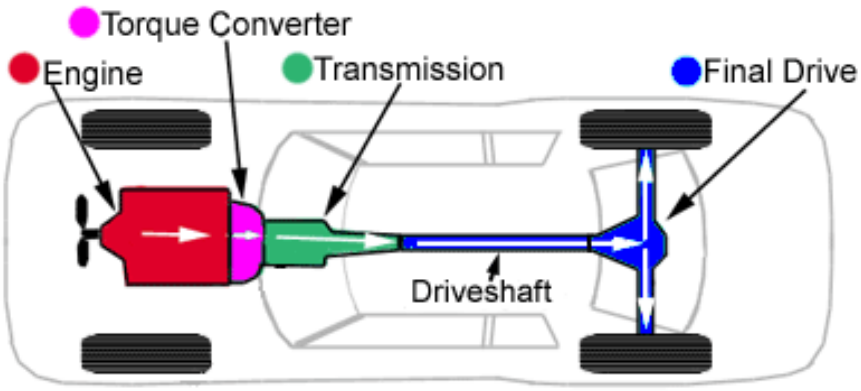

Fig. 1. Undercarriage view of rear wheel-drive system [8]

According to a 2012 study done by IHS Automotive, 46% of commercial vehicles utilize RWD or AWD [9]. Since Team DRIVE is focusing on incorporating hybrid technology into RWD and AWD vehicles, it is crucial to compare the advantages and disadvantages of RWD and AWD drivetrains when compared to the most popular form of drivetrain, FWD.

There are many advantages and disadvantages when comparing FWD, RWD, and AWD vehicles. One study, conducted by Tatsuro Muro (1997) of Ehime

University, compared traffic performances during driving and braking of a vehicle with two-axle AWD, RWD, and FWD running up and down a loose, sandy, and sloped terrain. The relationship between the effective tractive and braking effort, the total amount of sinkage of the front and rear wheel, and the slip ratio were all calculated throughout the experiment in order to determine the eccentricity about the central axis of the center of gravity of the vehicle [10]. The experiment concluded that during driving action, the maximum effective tractive effort of the AWD vehicle was larger than that of the RWD vehicle, which in turn was greater than that of the FWD [10] . The maximum terrain slope for which the two-axle wheeled vehicle is able to drive was found to be approximately 12 degrees for the AWD vehicle, 5.6 degrees for the RWD vehicle, and 3.1 degrees for the FWD vehicle, proving that AWD and RWD vehicles can perform on slopes where FWD vehicles struggle [10]. This experiment and its results can be used to show that AWD and RWD vehicles perform better in rougher terrain than FWD vehicles, thus making them safer and more appealing to consumers.

A different experiment was conducted by Stephen Hallowell and Laura Ray (2003) at Dartmouth College on all-wheel driving using independent torque control of each wheel. The experiment created situations where the driver was trying to accelerate on a straight road while the right rear tire was on ice [11]. The system transfers torque from the right rear tire to the right front tire, allowing the torque distribution system to behave as the driver desires in cases when, without the control system, it would not [11]. Due to an increase in driver control over the vehicle's motion, Hallowell and Ray concluded that by using the torque distribution system, driving performance and safety are improved. By simulating driving conditions on a variety of road conditions, the

researchers were able to apply their conclusion that AWD offers drivers more control to a wider scope of environmental conditions.

In conclusion, RWD and AWD vehicles offer a powertrain that increases vehicle handling and safety when compared to FWD vehicles. Therefore, it is crucial that regenerative braking technology be adapted to RWD and AWD vehicles. As a result, in order to improve the vehicle handling and safety of hybrid vehicles, the scope of hybrid vehicles must be expanded to RWD and AWD vehicles.

2.2 Electromagnetic Induction and Faraday's Law

Electromagnetic induction is the generation of an electrical current in a closed loop due to a changing magnetic field [12]. This property is described by Faraday's Law, as seen in Equation 1. Magnetic flux is defined as the amount of magnetic field passing through a given surface or area. The amount of voltage produced from electromagnetic induction is dependent on the number of coils and the rate of change of magnetic flux, $d\varphi/dt$. The negative sign indicates that the induced field opposes the change in magnetic flux as provided by Lenz's Law. The alternating voltage field generated by a rotating permanent magnet within a stationary copper wound stator can be found in Fig. 2. As seen in Fig. 2, the generated oscillating voltage field alternates between positive and negative voltages. Section 2.6 will explain how an oscillating voltage field can be converted into a non-oscillating positive voltage field. In Figure 2, electrical current is applied through windings surrounding the rotor, generating a magnetic field. As the rotor rotates within the stator, the fluctuations in the magnetic field induce an alternating current within the stator coils.

$$V = -N\frac{d\phi}{dt}$$

Equation 1. Faraday's Law. V represents the induced voltage, N the number of coils, t the time, and φ the magnetic flux

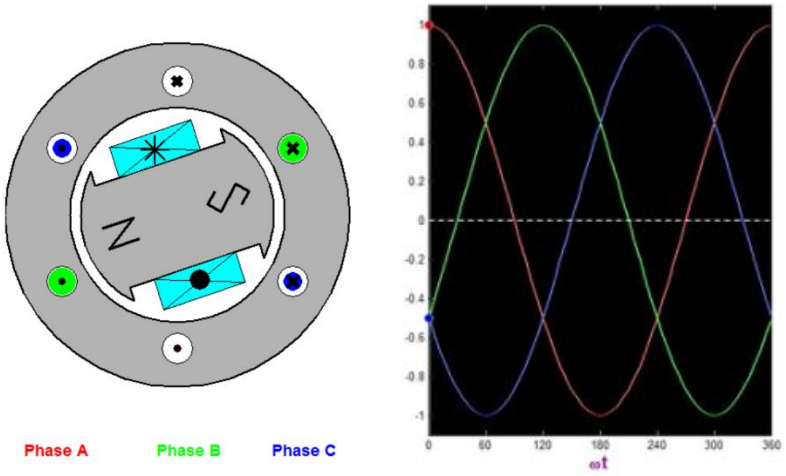

Fig. 2. Electromagnetic induction in a three-phase alternator. The graph on the right is a plot of the amplitude of each phase as the magnet is rotated [13].

2.3 Alternators: Generation of Alternating Current

Electromagnetic induction is a critical component in the generation of electricity and as a result, Team DRIVE has researched current technologies that utilize electromagnetic induction. The most common mechanical system that generates electricity in this manner is the alternator. Alternators come in a wide range of sizes and are commonly seen as generators on the industrial scale. Alternators are already found in cars and are responsible for recharging the car's battery [14].

The two main components found in alternators that are responsible for the production of alternating current, AC, are the rotor and stator. The Lundell rotor is the most common electromagnetic rotor found in car alternators [15]. Fig. 3 depicts a

Lundell rotor. Consisting of a rotating shaft, field coil winding, iron core, and two iron claw segments, the Lundell rotor is responsible for creating the changing magnetic field [14]. In car alternators, the field coil winding consists of 300-500 tightly wrapped coils of insulated copper or magnet wire wound over the iron core [14]. Current flows through the coils, which is controlled by a voltage regulator. By wrapping current-carrying copper wires around an iron core, a solenoid is created and thus an electromagnet becomes the source of magnetic flux. The two iron claw components channel the generated magnetic flux to the surface of the stator [14]. Since the current going through the coils is DC, North and South magnetic poles are created. In the design, the claw segments are interlaced and attached to the shaft, producing alternating North and South poles [14]. As the shaft rotates, the stators will experience alternating North and South poles, creating an overall AC style magnetic field [14].

Fig. 3. Lundell rotor from a disassembled automobile alternator

The stator serves as the component that is responsible for capturing the AC style magnetic field that is generated by the rotor. Also, the stator is responsible for

converting the mechanical rotation of the shaft into electrical energy. The stator consists of an iron core that surrounds the rotor. The iron core will complete the magnetic circuit between the rotor and stator [14]. The stator then has iron teeth that extend from the core and point towards the rotor poles. As these teeth are made of iron, the teeth provide another path to complete the magnetic circuit [14]. In the gaps between the stator teeth lie coils of copper wire. The alternating magnetic flux, generated from the rotor, induces a voltage in the coils. From this process, alternators can generate electrical energy from mechanical energy.

2.4 Alternator Efficiency

In order to quantify the results of the team's research, alternator efficiency must be measured to ensure sufficient net energy capture. Alternator efficiency is governed by the amount of energy lost, which can be distributed into three categories: mechanical, magnetic, and electrical.

The mechanical energy loss is due to friction between the shearing of air, exposed rotary components, and bearing fiction [14]. Assuming the use of a more common brush alternator, depending on the models available, there are frictional losses between the brushes and slip rings. However, these frictional losses are considered negligible, with significant friction losses due to the belt pulley system and windage. The friction in the belt pulley system is due to the contact between the belt on the pulleys at high angular velocities. The windage friction is due to the shearing of air with the rotating and moving surfaces. Both sources are then responsible for energy loss within the system. It is important to note that the belt pulley system is only present within an alternator located by the engine and would not be relevant at other major

locations within the powertrain and therefore won't be a source of power loss in the team's proposed regenerative braking system.

Magnetic losses incurred from material properties, such as flux density, are another form of energy loss and are directly proportional to output current [16]. The other source of magnetic loss, eddy currents, is dependent on the metallic plate thickness in the stator, as thicker plates lead to the creation of more eddy currents. All of these magnetic considerations then account for the design of the electromagnet and pole configurations of alternators. For instance, the popular permanent magnet 12-pole configuration within Lundell alternators presents a compromise between increased electrical output and increased magnetic power loss [16].

The electrical energy loss presents the greatest source of inefficiency within existing technologies. As previously stated, the most common alternator currently used in commercial automobiles is the Lundell alternator [15]. Despite being considered the optimal choice, the Lundell model yields low power output and is seen only as the best compromise between cost and efficiency [17]. With the increase in power demand of automobiles from 1 kilowatt to 2.5 kilowatts since 1985, the performance level of the Lundell design cannot keep up with trends in energy consumption [15]. Power output could be greatly improved by minimizing electrical energy losses in the alternator. Electrical energy lost through the stator windings is the most significant loss of efficiency within Lundell alternators [16]. Experimental studies suggest that changing the number of stator windings can optimize efficiency in the alternator [16].

2.5 Rotor Construction

There are two main components of an electromagnet: the ferromagnetic core and magnet wire windings. The choice of core material will impact the overall efficiency and power output of the alternator. The material properties that will be considered when deciding on the core material are permeability, saturation, coercivity, remanence, and resistivity. For the team's alternator application, a material with high permeability and saturation, and low coercivity, remanence, and resistivity would be most suitable. High permeability was desired because a core that would reach peak magnetic flux more quickly would allow for an increase in the generation of electrical power. High saturation was required because we wanted the core to maintain the greatest magnetic flux possible. Low coercivity was desired because we wanted the magnetic flux to return to its lowest levels with the least amount of an applied magnetic field. Low remanence was desired because the team wanted a core that would have as little remaining magnetic field when the rotor was deactivated so that there would be no stray effects. Low resistivity was desired because the team wanted a core that resisted an imposed electric field as little as possible. High purity iron matches these properties and therefore will be considered as the core material for the rotor [18].

Regarding the individual components of the alternator, the choice of magnet wire influences power output. Magnet wire is the thin, insulated copper wire coiled around the iron core in the rotor and nestled within the stator teeth [14]. Due to the voltage loads, physical windings, and high temperature, the insulation undergoes degradation and can lead to motor failure [19]. Insulation generally deteriorates logarithmically with respect to increasing temperature [19]. Insulations are categorized

by thermal grades, where a 200 °C thermal grade will degrade after 20,000 hours at 200 °C, and a 180 °C thermal grade insulation will degrade after 5,000 hours at 200 °C [20]. Magnet wire with sufficient thermal insulation will be selected for rotor configuration to avoid motor failure within the alternator and ultimately improve efficiency.

The shape and size of the rotor will also influence power output. As the rotor turns within the stator, electricity is produced to power the electrical components. The pole arrangement and the size of the poles strongly influence the electromagnetic force produced by the electromagnet [21]. Finding an effective shape for the rotor maximizes the amount of force produced by magnetic flux. Maximizing the force helps produce the most power possible. The two main types of rotor configurations for electrical generation in the field are the salient and cylindrical cores [22]. A simple diagram of a salient rotor is shown in Fig. 4 and a simple diagram of a cylindrical rotor is shown in Fig. 5.

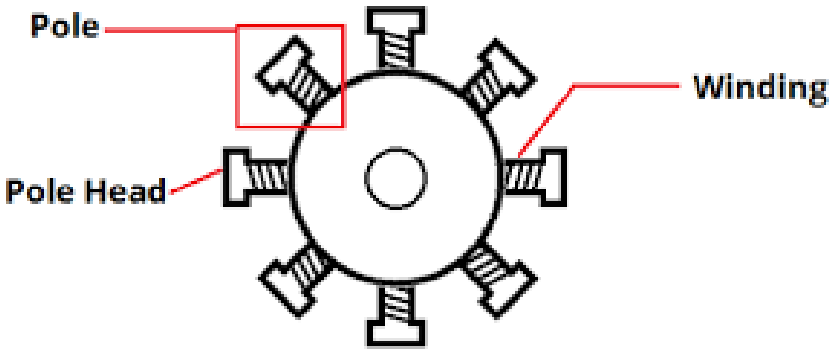

Fig. 4. Eight pole salient rotor [23]

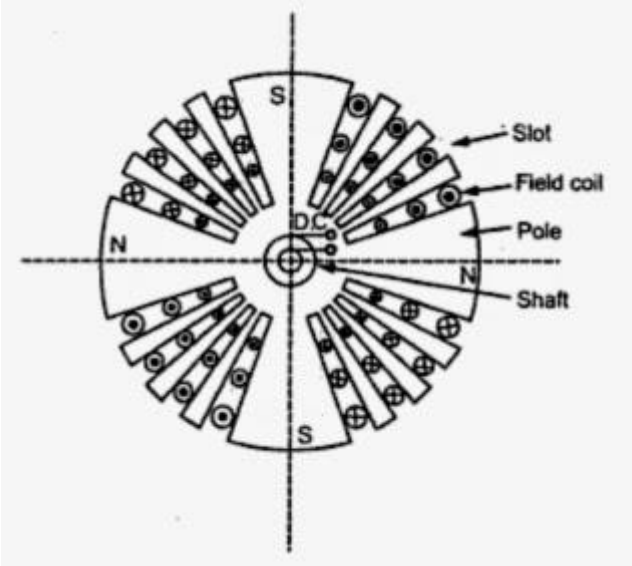

Fig. 5. Wiring diagram of a cylindrical rotor [24]

The salient pole rotor features multiple magnetic poles with a field coil winding around each individual core. Each pole then produces its own local magnetic field that interacts with the stator coil to produce an electrical output. The cylindrical pole rotor, alternatively, has slots along the cylindrical face in which the coil windings rest. As the salient pole rotors operate at lower revolutions per minute (RPM), they require more poles to achieve a sufficient frequency output; a typical salient pole rotor has anywhere from 4 to 60 poles while a cylindrical rotor could expect 2-4 poles [25]. From a mechanical perspective, the salient configuration has a larger diameter to length ratio than the cylindrical as well as a less structurally sound shape due to its rotational inertia. Salient rotors are typically used for RPM ranges of 1500-3000 RPM and cylindrical rotors are typically used for RPM ranges of 125-500 RPM, indicating that salient rotors would be best used for a drive shaft, since drive shaft RPMs at driving speeds can reach 2300 RPM [24]. Each core shape is then optimized for its particular application.

An alternative to these is the Lundell rotor, or a claw-pole configuration. This rotor design consists of a single field coil surrounded by multiple interlocked core pieces and acts as a synchronous generator [26]. The Lundell rotor is the predominant choice for automotive alternators and can be outfitted for a wide range of vehicle types and load cases: for instance, an increase in the number of poles would be apt for use in trucks and busses where more output power is needed. However, a weakness of the Lundell rotor is its efficiency; as it averages around 50% efficiency at peak speeds and loads [27]. Its benefits and prevalent use derive from its low cost and versatility, because it has been seen as the norm for automobiles.

2.6 AC/DC Conversion

As mentioned before, alternators and similar technology generate an alternating current. However, batteries can only be recharged by direct current. With this constraint, Team DRIVE must investigate efficient ways in which alternating current can be converted into direct current to maximize the overall efficiency of the system. Although there are several ways to go about this process, the most efficient and widely used is the three-phase charging system. This method uses three charging coils in the alternator and has the alternating current cycles of each coil offset by 120 degrees so that at every point in the cycle, one of the currents is at or near its maximum value [28]. These coils are then connected to a rectifier containing six diodes, as seen in Fig. 6. This method is ideal because after the alternating currents have been converted to a direct current, the result is a relatively flat and steady current instead of a pulse, shown in Fig. 6 [28]. Although the three-phase charging system is very efficient in comparison

to other systems, it still loses a significant amount of energy in the form of heat. At maximum speeds, a rectifier on the alternator of an automobile can reach 200 °C [29].

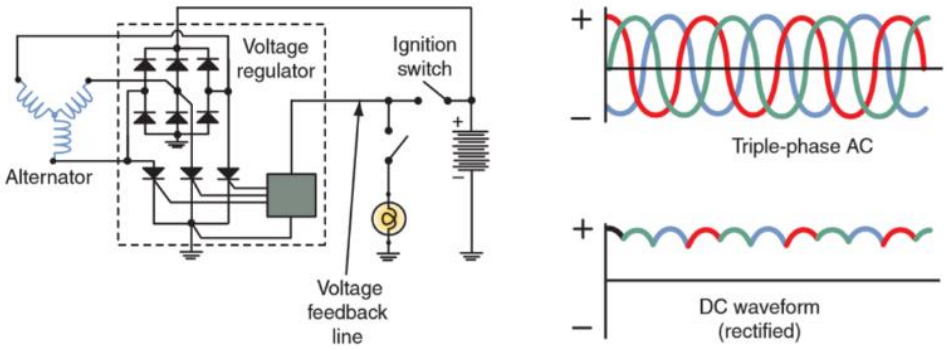

Fig. 6. Three phase rectifier and diagram of resulting current [28]

2.7 Regenerative Braking

To provide context for the technology proposed, Team DRIVE conducted research on existing regenerative braking technology. When a car uses a traditional braking system, any mechanical energy that is dissipated from this action is converted into heat, which is then lost and wasted. However, in a hybrid or electric vehicle, 8-25% of that wasted energy can be saved to charge the vehicle's battery through the use of regenerative braking [30]. To implement regenerative braking, the motor acts as a generator, converting kinetic energy into electrical energy, which is then stored in a battery [30]. When the brakes are applied, the electric motor acts in reverse to slow down the vehicle, allowing the motor to function as a generator [30]. At the same time, the brake controller monitors the wheel speed and calculates both the torque required to halt the wheel and the amount of excess energy from the rotational force of the wheels that can be converted to electricity. This electricity is transferred back to the battery [30]. Regenerative braking not only improves efficiency and conserves energy, but also reduces brake pad wear and fuel consumption, with more effectiveness in stop-

and-go driving environments [30]. If this braking process or similar implementation is further improved and utilized to its full potential, it is possible that more electric and hybridized vehicles could be present on the roads.

2.8 Conclusion

Despite the current advancements in hybrid technology, the automotive field could benefit from an expansion of this technology into RWD and AWD vehicles. The drive shafts of these RWD and AWD vehicles serve as an excellent source of underutilized mechanical energy. Besides offering better safety and handling, applying regenerative braking technology to AWD and RWD vehicles has the potential to drastically alter the current market for hybrid vehicles, improve the carbon footprint of the average driver, and reduce fossil fuel dependency. The literature has affirmed that alternators are an effective way of generating electrical energy and could serve as the core of the team's regenerative braking system. However, current alternator rotors show weaknesses in power efficiency at certain speeds, leading the team to believe that a more optimal alternator rotor can be used for an alternator-based regenerative braking system. The methodology section describes how Team DRIVE proceeded throughout the research process in conducting experiments to determine a design that maximizes the energy output of an alternator placed along the drive shaft.

Chapter 3: Methodology

3.1 Sub-Teams

To carry out the research, the members of Team DRIVE were split into four sub-teams: software simulations, rotor design, data measurement, and test rig construction. The software simulations sub-team was responsible for running simulations in ANSYS Maxwell, an electromagnetic field simulation software, and performing analyses on the magnetic flux data obtained. The rotor design sub-team was responsible for designing prototype salient rotors, creating CAD models of the rotors, and analyzing the data to aid with the creation of new rotors for simulation. The data measurement sub team was responsible for designing and implementing the sensor setup that collects data from experiments done with the test rig. The test rig construction sub-team was responsible for constructing and maintaining the test rig such as fitting the prototype alternators to the test rig.

3.2 Variables

In order to improve the two dependent variables, power output and braking torque, of existing alternators, the team manipulated the rotor type and geometry to test for increases in power output and efficiency. The overarching dependent variables that were used to evaluate efficiency were power output and braking torque. In addition, change in heat output was measured as it directly correlates to change in efficiency, however, it is not one of the main dependent variables. Instead, the data collected from measuring heat output provides the team with an estimate of the effectiveness of any manipulated variables; if the heat generated from a 4-pole rotor constitutes a greater portion of the overall power output than an 8-pole rotor, then it will be deemed as less efficient.

To observe potential changes in the dependent variables' efficiency, two independent variables are tested: alternator rotor type and alternator rotor geometry. The Lundell rotor served as the control rotor type and control rotor geometry because it is the most common alternator rotor. There were two tested rotors, a 4 and 8-pole salient rotor. As stated before, the greater the number of salient poles, the greater the efficiency at lower RPMs, therefore 4-pole and 8-pole salient rotors would offer a better glimpse at salient rotor efficiency for a wide range of RPMs. Furthermore, comparable studies of rotors with numerous poles in an AC induction motor reveal that 4-pole rotors perform better [31]. Too small a pole number increases flux density within the poles and can saturate the path. On the other hand, a rotor with 8-poles was chosen to maintain the even numbering and observe effects at higher pole values. Maxwell simulations were used to determine the optimal rotor geometry for each salient rotor. The optimal 4 and 8-pole rotors were then recommended for future testing and implementation into an alternator-based regenerative braking system. Potential extraneous variables that may arise for each independent variable are discussed in the specific sections for the variables.

3.3 Dependent Variables

3.3.1 Power Output

As the purpose of this device is to recover wasted mechanical energy as electricity, the main dependent variable of this study is power output, which is directly related to the overall efficiency of the combination of rotor type and rotor geometry. Digital ammeters and voltmeters with serial outputs will measure power inputs and outputs from the alternator.

3.3.2 Braking Torque

The braking torque generated by the alternator is the next dependent variable measured in the experiment. In order to test this, the team will have the alternator mounted on the previously described test rig. The team will use the DC driver, or motor, and pulley system to drive the test shaft at an angular velocity close to that of an automobile's drive shaft at highway speed, usually between 1900 and 2300 RPM [32]. All experiments will begin with an initial RPM of 2300 RPM. Before the electromagnet is initiated, the team will record the initial RPM and torque using the TRS500-FSH01992 Rotary Torque Sensor. Then the electromagnet will be initiated for a short, predetermined time. At the instant when the electromagnet is initiated, the DC driver will slowly decelerate at a constant and controlled rate, in an attempt to mimic the action of braking, which will be called the "braking phase". The change in torque will then be recorded. After the time period has ended, the electromagnet will be deactivated and the DC driver will return to driving the rotor back to the original RPM. Whenever the electromagnet is not activated, the system will be in the "driving phase."

This cyclic loading will occur many times in an attempt to mimic driver/vehicle behavior. Also, in order to establish a baseline to evaluate whether the alternator can act as a braking system, the DC driver will decelerate at the same rate as before and for the same duration of time as the activated period of the electromagnet. The data collected from this cycle will represent a control group where any changes from the created baseline will indicate that the alternator was acting as a secondary braking system. The main extraneous variable present will be passive resistance of the drive shaft system. For example, once the "braking phase" has occurred, any type of passive

resistance, mainly friction from contact or lack of lubrication, can cause the drive shaft to decelerate even further, which can then skew the results of how the alternator performed as a secondary braking system. The team will account for this by running the shaft at different speeds without powering the alternator to determine the resistive torque of the system at each speed and develop a function to estimate the contribution that the system's passive resistance makes to the shaft's deceleration.

3.4 Independent Variables: Rotor Type and Geometry

The team will test two different rotor types against the Lundell rotor control group, a 4-pole salient rotor and an 8-pole salient rotor. The main independent variable of this study is the rotor geometry. The reason for choosing different types of salient rotors is due to the range of angular velocities that the drive shaft and alternator prototype will be operating in. Fig. 7 shows the overall efficiency of a Lundell alternator at varying operating angular velocities, with a peak efficiency of 55% at approximately 1500 RPM [16]. As mentioned earlier, the maximum angular velocity of a drive shaft can reach 2300 RPM. However, during the braking process, the drive shaft and alternator prototype will be experiencing a range of angular velocities, from 2300 RPM, at the onset of braking, to 0 RPM, when the car has come to a complete stop. Due to the drop in Lundell rotor efficiency at angular velocities lower than 1500 RPM, the efficiency decreases by 15% from 1500 RPM to 1000 RPM, representing a 27% loss of relative efficiency.

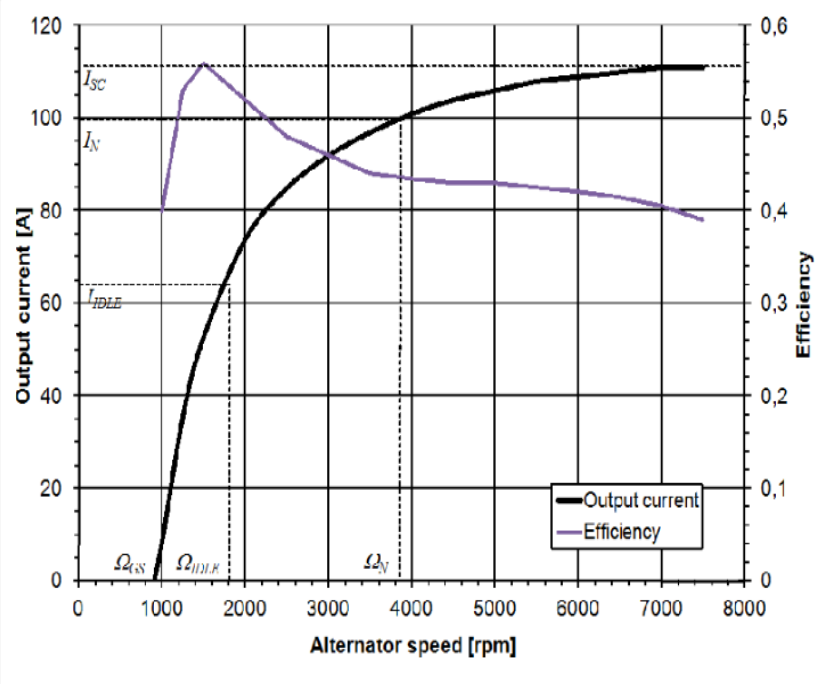

Fig. 7. Efficiency of a Lundell alternator [16]. A decrease in efficiency is observed for RPMs less than approximately 1500 RPM.

As mentioned in Section 2.5 salient poles operate more efficiently at lower angular velocities. Therefore, the 4-pole and 8-pole rotors are considered in an attempt to avoid the decrease in efficiency that Lundell rotors experience at angular velocities below 1500 RPM. A possible extraneous variable that can lead to misleading efficiency results includes possible inconsistencies in molding. When a ferromagnet is exposed to high temperatures, the magnetic domains of a ferromagnet can become scrambled, leading to a decrease in the maximum possible magnetic flux density. During the molding process, the magnetic domains of the material can be scrambled to an even higher degree, leading to a decrease in magnetic flux density when used as an electromagnet [12].

In order to determine the ideal prototype design, ANSYS Maxwell was used to simulate the alternating magnetic flux generation for a variety of rotor prototype designs. ANSYS Maxwell will be described in further detail in Section 3.6. To reduce the number of potential prototype designs that needed to be tested, Design of Experiment, DOE, was used to reduce the number of prototypes that were tested in ANSYS Maxwell. As seen in Fig. 8, there are 4 different geometric variables that were tested. With 4 different factors, 2 levels, high and low, were designated for each factor. Therefore, there would need to be 16 different Maxwell simulations. However, with only 2 levels, it would be difficult to produce a mathematical relationship from the 4 different geometric factors.

Ideally, three levels for each factor would be sufficient, but 3 levels for each of the four factors would mean there would need to be 81 preliminary Maxwell simulations which isn't feasible. Therefore, the team made another assumption to reduce the number of simulations. The inner diameter, D_i, would remain fixed at the diameter of the central rod of the Lundell rotor, 16.87 mm, used in the study. This smaller diameter would increase the number of windings, improving power output. The wire diameter was selected to be 0.85 mm for each winding because it was the same diameter as the magnet wire found on the Lundell rotor used in the study. For both the 4-pole and 8-pole rotors, the rotor was extruded to a depth of 43.55 mm, the depth of the Lundell rotor used in the study.

Another assumption made was that the head height, H_h, is dependent on the pole height, P_h, and the outer diameter of the Lundell rotor used in the study is constrained

to 90 mm. As a dependent variable, H_h is not a potential factor that can be incorporated into the DOE evaluation. However, pole thickness, $P_{t,}$ will be considered as a factor. With 2 factors and 3 levels for each factor, there would be a total of 9 preliminary Maxwell simulations. Table 1 shows the DOE factors for the first preliminary experiments of the nine 4-pole rotors. Table 2 shows the geometric dimensions and number of windings for each of the preliminary 4-pole rotors. Windings were represented as a rectangle that was swept around each pole. Winding number was then determined by assuming hexagonally packing within a rectangular cross section of the simplified winding geometry.

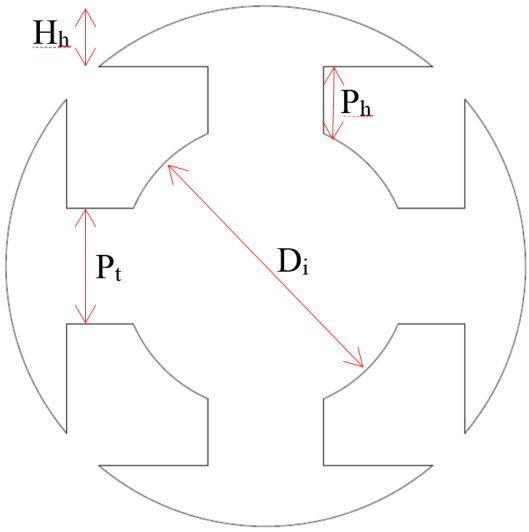

Fig. 8. Salient rotor geometric variables

Factors	**Minimum**	**Intermediate**	**Maximum**
P_h	23.385 mm	29.975 mm	35 mm
P_t	5 mm	10.935 mm	16.87 mm

Table 1. DOE factors and levels of preliminary 4-pole rotors experiment

#	**1**	**2**	**3**	**4**	**5**	**6**	**7**	**8**	**9**
P_h	23.4	23.4	23.4	30	30	30	35	35	35
P_t	5	10.9	16.9	5	10.9	16.9	5	10.9	16.9
W	189	29	26	245	37	34	284	43	39

Table 2. Preliminary 4-pole rotor dimensions

Table 3 reflects the factors manipulated for the 8-pole rotor iterations. With 8 poles surrounding the inner circle, there is a limitation to the maximum pole thickness possible. Thus, the maximum 6.456 mm thickness is derived as anything larger leads to interference of pole ends and the creation of a larger inner diameter. The minimum thickness value chosen, 4 mm, is reflective of machining capabilities. The chosen machining technique of wire electrical discharge machining (EDM) can create pieces with tolerances of +/-0.002 inches or 0.0508 mm [33]. For professional CNC milling, recommended nominal part thicknesses are on the order of 1.02 mm [34]. Regardless of this level of precision, a larger thickness is required for structural rigidity and support. For the initial round of testing, a rough minimum 4 mm thickness was chosen. The intermediate thickness value is then just the middle increment between the minimum and maximum chosen thicknesses. Note that the 4 mm thickness ensures that at least 1 mm of difference is allowed between iterations. Any smaller of a thickness would exacerbate the experienced displacements and stresses in the poles. This can be confirmed by a finite element analysis conducted on a sample 8-pole rotor with a 4 mm pole thickness. The results of an applied centrifugal force of 2100 RPM are shown in Fig. 9.

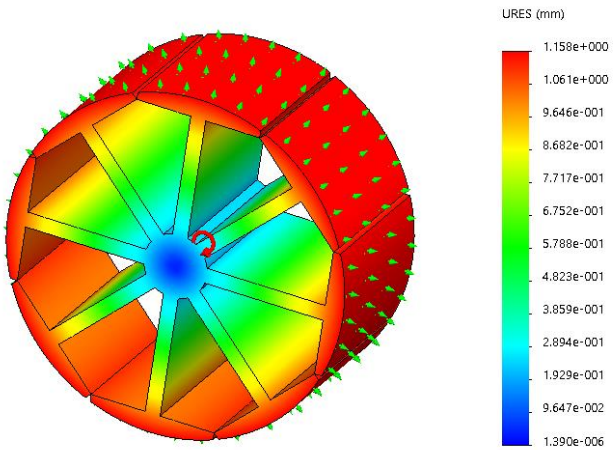

Fig. 9. Finite element analysis of a sample 8-pole rotor

Factors	**Minimum**	**Intermediate**	**Maximum**
P_h	26.565 mm	29.065 mm	31.565 mm
P_t	4.000 mm	5.228 mm	6.456 mm

Table 3. DOE factors and levels of preliminary 8-pole rotors experiment

The head heights chosen follow a similar methodology. The minimum head height is 5 mm based on the constrained radial length and corresponding to the maximum pole height of 26.565 mm. This is 1 mm larger than the minimum thickness chosen seeing as the head tapers off at the ends of its arcs and has a smaller average thickness. The dimensions reported are only the maximum thickness of the sector of the pole head. Even increments of 2.5 mm were chosen with a maximum head height of 10 mm and intermediate value of 7.5 mm. These correspond to the shown pole heights of 29.065 and 31.565 mm. Any larger of a head height and the head significantly surpasses the pole thickness and increases the rotational inertia of the pole.

Based on the two dimensions and three different values, there are a total of 9 preliminary iterations. The rotor numbering scheme and dimensions are detailed in Table 4 for the 8-pole rotors. These dimensions and numbering scheme remain constant for the simulations except where detailed in the results.

#	1	2	3	4	5	6	7	8	9
P_h	31.6	29.1	26.6	31.6	29.1	26.6	31.6	29.1	26.6
P_t	4	4	4	5.2	5.2	5.2	6.5	6.5	6.5
H_h	5	7.5	10.0	5	7.5	10	5	7.5	10

Table 4. Preliminary 8-pole rotor dimensions

Based on the dimensions for the rotor core, the 8-pole winding dimensions can be decided. Table 5 reflects the number of layers of winding around the pole (L), the number of stacked windings along the height (S), and the total number of windings (W). Similar to the 4-pole rotors, hexagonal packing was initially chosen to maximize the number of windings. However, due to the fewer number of winding layers fit around the individual poles, rectangular packing was found to be more efficient. Whereas the 4-pole iterations had more clearance between rotor poles, the 8-poles suffer from tight packaging at the pole ends closest to the yoke. The greater number of poles fit around the inner diameter then lead to a maximum of 3 layers of windings around a single pole. This packaging was designed assuming a winding layer spanning the maximum possible length of the pole, or its P_h.

#	1	2	3	4	5	6	7	8	9
L	3	3	3	3	3	3	2	2	2
S	34	31	28	32	29	26	33	30	27
W	102	93	84	96	87	78	66	60	54

Table 5. Winding characteristics of preliminary 8-pole rotors

3.5 Salient Rotor Testing

As previously discussed, there will be a control rotor and two experimental rotors. The Lundell rotor underwent test rig experiments and a 4-pole and 8-pole salient rotor was recommended for use within an alternator-based regenerative braking system. Since the team made no modifications to the Lundell rotor, the procedure for test rig experiments will be straightforward. However, the two experimental rotors

required optimization. As discussed in Section 3.5, the dimensions of each 4-pole and 8-pole rotor set will be assigned based on a DOE approach, but a method is still required to predict the braking torque and power output of each 4-pole and 8-pole prototype rotor. In order to reduce the number of test rig experiments, the team will optimize the geometric features of the 4 and 8-pole salient rotors using ANSYS Maxwell simulations.

ANSYS Maxwell software is designed for rendering 3D magnetic fields of electromagnets and permanent magnets, for the salient rotor simulations. Using the software, the team manipulated the dimensions of the different rotor shapes that were tested in order to maximize the magnetic field at specified radii. These specified radii were the distance from the rotor to the stator coils. The specified radii varied from alternator to alternator, meaning that they cannot be determined until the alternator has been purchased and disassembled. For the simulations, a single radius was used and was determined from one of the alternators the team acquired. Since electromagnets were simulated, a single type of magnet wire was wound around the rotor shapes to create a solenoid, and therefore an electromagnet. By doing this, the team hoped that the simulation data would help guide future research and reduce test rig experimentation time.

3.6 Simulations

Through the use of ANSYS Maxwell, Team DRIVE has tested multiple rotor shapes in order to determine the magnetic field generated by an excitation current and simulated the induced current in the stators. These rotors varied in number of poles, thickness, length, and number of windings in the excitation coils. The goal of this

process was to optimize these parameters in order to produce the greatest power output from the induced current.

Each rotor design was modeled in Autodesk Inventor and SolidWorks and imported into ANSYS Maxwell. Fig. 10 depicts a rotor created in Autodesk imported into an ANSYS Maxwell workspace. Each model consisted of both the rotor core and excitation coils. Although each coil would consist of multiple windings in real life, a revolved rectangle was used to depict each coil in order to simplify the simulation process. Using the material library in ANSYS Maxwell, the rotor core was assigned as iron and the excitation coils were assigned as copper because they are the most common materials used for their respective part. Each coil was assigned an excitation current of 7 mA, the excitation current of the Lundell alternator, multiplied by the number of windings. The direction of the excitation current was chosen such that the poles would alternate from north to south. A vacuum region was defined around the model with a 60 mm offset from the origin in every direction. These dimensions were chosen because they encapsulated the entire stator, allowing the team to view the magnetic field data relevant to the induced current. Each simulation was run with 10 passes with an allowed error of 1%. Upon completion of the simulation, a visual representation of the magnitude of the magnetic field vectors throughout the vacuum region was generated using a logarithmic scale. Additionally, a similar visual representation of the magnitude of the magnetic field vectors on the surface of the rotor core was generated. These images allowed for a qualitative analysis of the magnetic field and allowed Team DRIVE to better understand how the rotor shape was affecting the magnetic field.

Finally, the magnetic field vector data for each point throughout the control region was exported in the form of a text file for quantitative analysis.

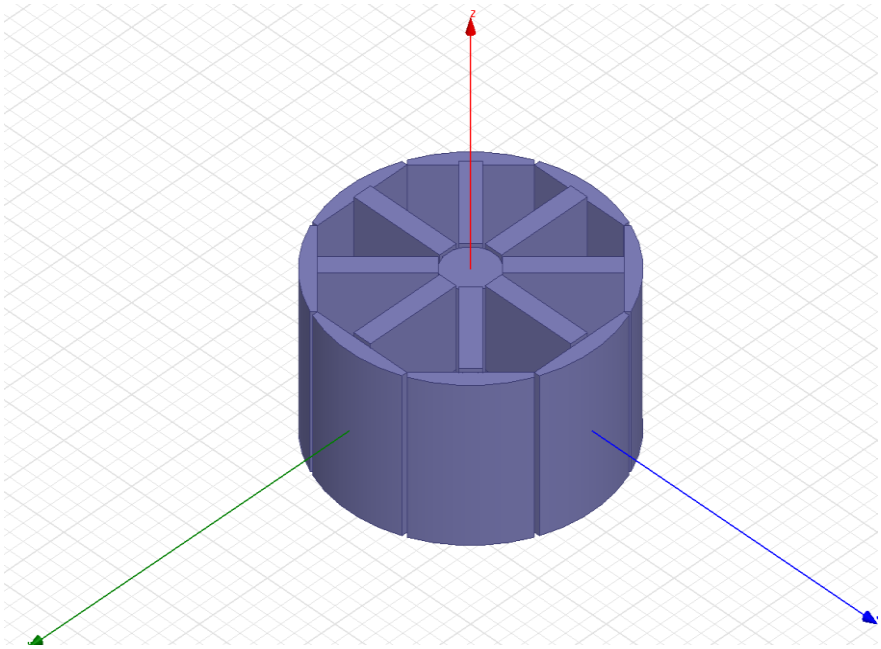

Fig. 10. A STEP file of a rotor core prior to simulation in ANSYS Maxwell

Once the data has been exported to a text file, it is then imported into a MATLAB script. This script processes the data and converts it into useable information. The output of the script is the voltage, current, and power values at specified rotational velocities in the region that would be occupied by the stator coils. The script first filters out points that are not in the region, then sums up the magnetic field values at points within that region. Ideally, these sums would be sinusoidal in nature, as seen in Fig. 11, and from there the magnetic field data can be converted into voltage and current. Several plots of the data as it is being processed is also outputted

by the script, showing the different stages in the script and allowing for qualitative assessments of how closely the data aligns with the model.

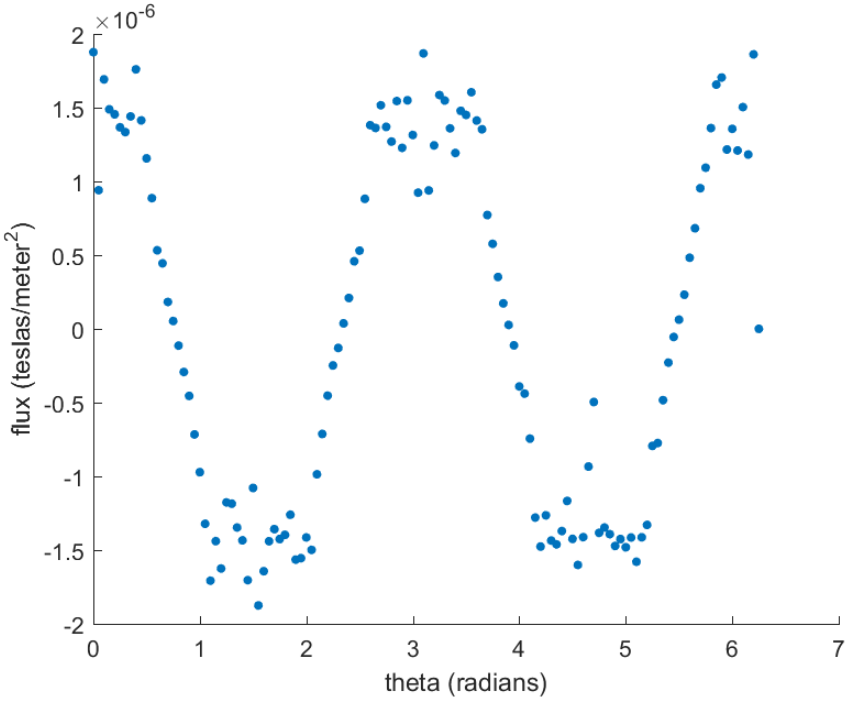

Fig. 11. Magnetic flux as a function of position, denoted by the angle theta, calculated based on ANSYS Maxwell data and interpreted using MATLAB

3.7 Test Rig

After all simulations were completed using ANSYS Maxwell, test rig experiments could be undertaken. To conduct the experiment, the test rig sub-team constructed a test rig using the CAD model shown in Fig. 12. The rig consisted of a DC driver that connects to the steel shaft via roller chains and sprockets. However, the DC driver has a max speed of 1750 RPM, while a typical automotive drive shaft rotates at speeds between 1900 RPM and 2300 RPM. To account for this, the selected sprockets have a tooth ratio of 21:16, allowing the simulated drive shaft's max speed to reach a speed comparable to the max speed that typical vehicular drive shafts

experience. Fig. 13 shows a more comprehensive look at the portion of the test rig containing the drive shaft.

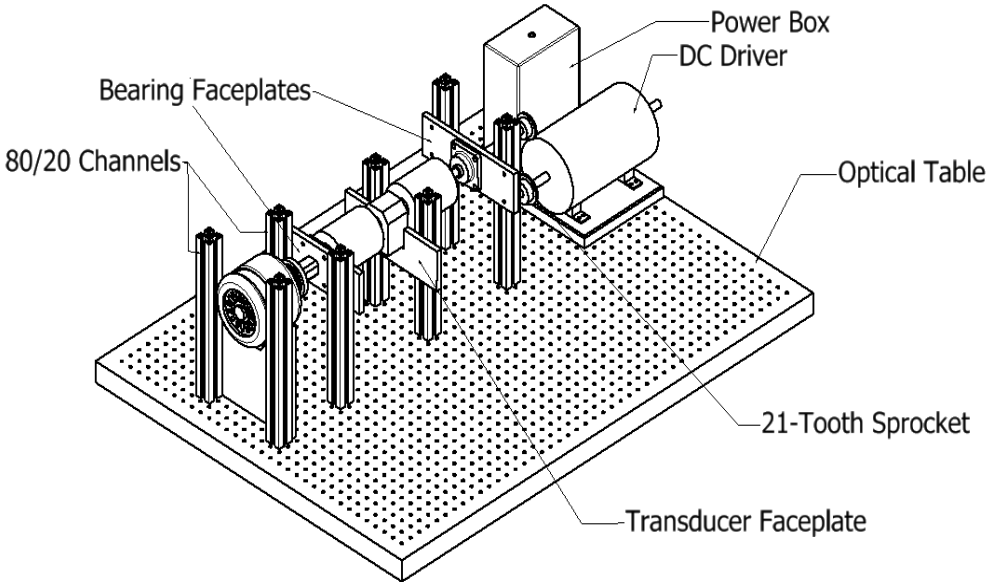

Fig. 12. CAD model of test rig

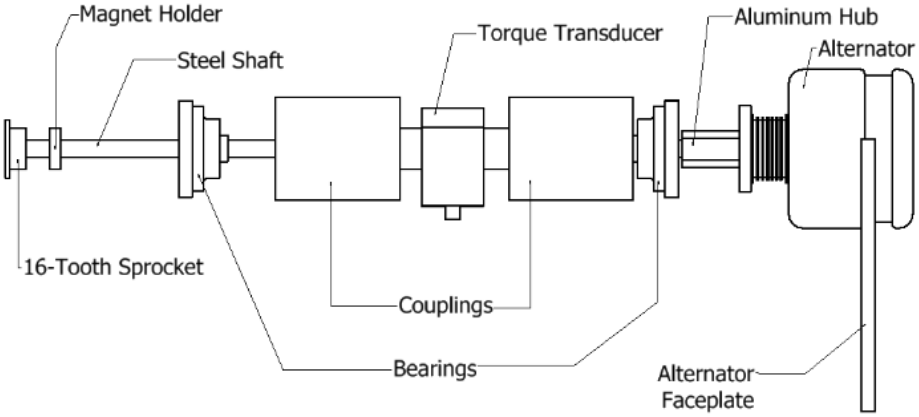

Fig. 13. CAD model of drive shaft section of test rig

As seen in Fig. 13, the 16-tooth sprocket was attached to a steel shaft which was supported by a bearing. This shaft was then coupled to one end of the torque transducer. The other end of the torque transducer was coupled to an aluminum coupling hub made specifically by the team so that the transducer could be coupled to

the alternator. The coupling hub had a wider base diameter than the coupled portion, allowing it to be bolted to a pulley that itself was bolted to the alternator. This allowed the torque to be transferred seamlessly through the aluminum coupling piece from the alternator to the torque transducer.

Lastly, for safety precautions, the team contained the test rig inside a cage in which the experiments took place. The cage, shown below in Fig. 14, had a metal frame that was covered by plywood on all faces except for the floor. The front side of the cage had a door that would be opened when modifications needed to be made but remained closed during testing. To secure the door, a standard door lock was used to keep the door shut. As extra protection, two wooden latches were located on either side of the door that held a bar in place to barricade the door. The entire cage sat on an optical table that allowed the test rig components to be secured during experimentation.

Fig. 14. Test rig cage

The TRS500-FSH01992 Rotary Torque Sensor from Futek is the torque transducer that was used within the test rig. This transducer model can measure torques up to 500 N-m, which covers the range of values that the simulations predicted. As seen

in Fig. 12, the transducer was seated in a slot that was cut in an aluminum plate. This kept the middle of the transducer stationary relative to the shafts on either side, allowing for proper torque measurement.

Fig. 15 shows the wiring schematic for powering the alternator. The Lundell model alternator used for testing was a 3G alternator with an “ASI” plug internal regulator. Based on the wiring necessary for this particular model, the vehicle loads of ignition, accessories, and other were replaced with the resistance network. Rather than power separate electronics, the power generated from the alternator in this study was then dumped across a separate load. As a result, the only power source needed was to provide the initial current to power the solenoid. This power source is typically rated at 12 V and is wired with a typical warning lamp in most vehicles. Based on other literature, an alternator driven at 2100 RPM may draw 0.15 A at most during startup [35]. Other necessary connections include rerouting a regulator wire back into the positive terminal of the alternator and routing a wire from the regulator to the stator coil. Finally, the alternator casing served as a ground for the device which can then be made common with the other grounds.

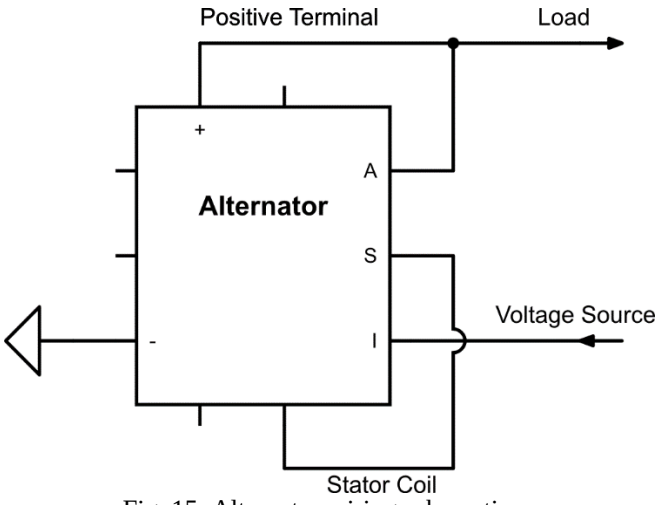

Fig. 15. Alternator wiring schematic

3.8 Sensor Configuration

During testing, the team will need to measure the current and voltage output of the alternator, the temperature of the alternator rectifier, the RPM of the rotating driveshaft, and the braking torque of the alternator. The team's procedure for measuring each of these parameters is discussed below using circuit diagrams.

Fig. 16 shows the team's setup of the temperature sensor within the test rig. The temperature sensor shown is a 700 series Platinum Resistance Temperature Detector (RTD) purchased from Digikey Electronics. This RTD was chosen for the test rig because it offers high accuracy and a very high thermal threshold while maintaining a linear relationship between resistance and temperature measured during the expected range of temperatures for the rectifier of the alternator. The resistance of the RTD increases as the temperature increases so the team has developed a custom LABVIEW virtual instrument (VI) to condition the voltage signal received from the RTD into temperature readings in Fahrenheit at a data rate of 1 Hz during the experiment.

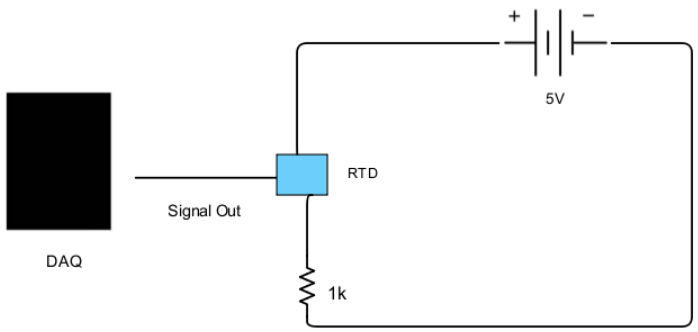

Fig. 16. Temperature sensor schematic

Fig. 17 shows the setup of the RPM measurement schematic that the team will utilize during experimentation. The sensor shown in Fig. 17 is a Hall effect sensor which detects magnetic fields. The Hall effect sensor will be placed on a stationary mount within the test rig that will keep the sensor a few centimeters away from the driveshaft within the test rig. A 3D-printed circular mount was designed to encase 6 evenly-spaced high-strength magnets, each with a 0.5 in diameter. The magnet mount is placed on the driveshaft directly so that it rotates at the same rate as the rest of the test rig and is placed in line with the Hall effect sensor. Every time the South pole of a magnet passes the Hall effect sensor, the voltage signal of the sensor drops to 0 V. Over the course of the test, the Hall effect sensor will output a square wave signal that the team will condition through LabVIEW to divide the number of peaks within a specific time interval by 6 to obtain the RPM reading. Six magnets are used in this setup to increase the resolution over a wide operating voltage range and was specifically designed by Adafruit for automotive applications, making it an ideal choice for the team's test rig. The RPM measurement will be compared to those of a digital tachometer to ensure accuracy.

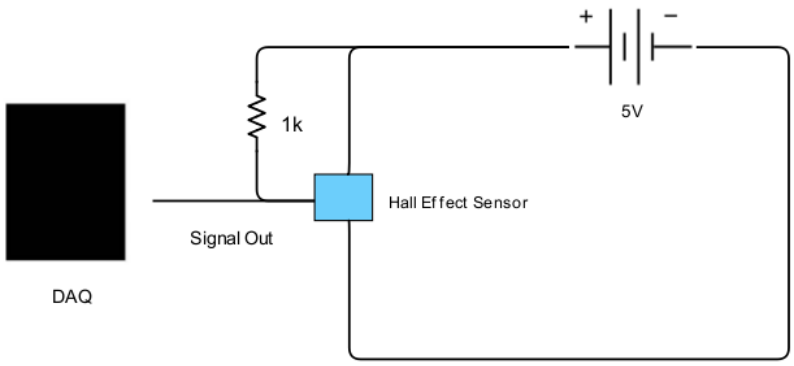

Fig. 17. RPM sensor schematic

Fig. 18 shows the current and voltage measurement circuit diagram to measure the power output of the alternator while testing. The current sensor used in the team's setup is an in-line, hall-effect-based linear current sensor produced by Allegro MicroSystems which features high isolation and accuracy for a wide voltage range and a low internal resistance of 100 μΩ. The current that passes through a series of copper coils within the sensor generates a magnetic field which is converted to a proportional voltage and outputted to the Data Acquisition System. The team has utilized LabVIEW to condition the voltage signal into a current reading using a linear conversion scale provided by the manufacturer. The current output of the alternator will then pass through a circuit of high-power resistors each with a resistance of 0.25 Ω to provide a total resistance of 0.1 Ω. This very low effective resistance value is needed because the team expects a maximum voltage and current output of approximately 14 V and 100 A and therefore it is necessary to minimize voltage that is dropped across the resistors in the voltage divider.

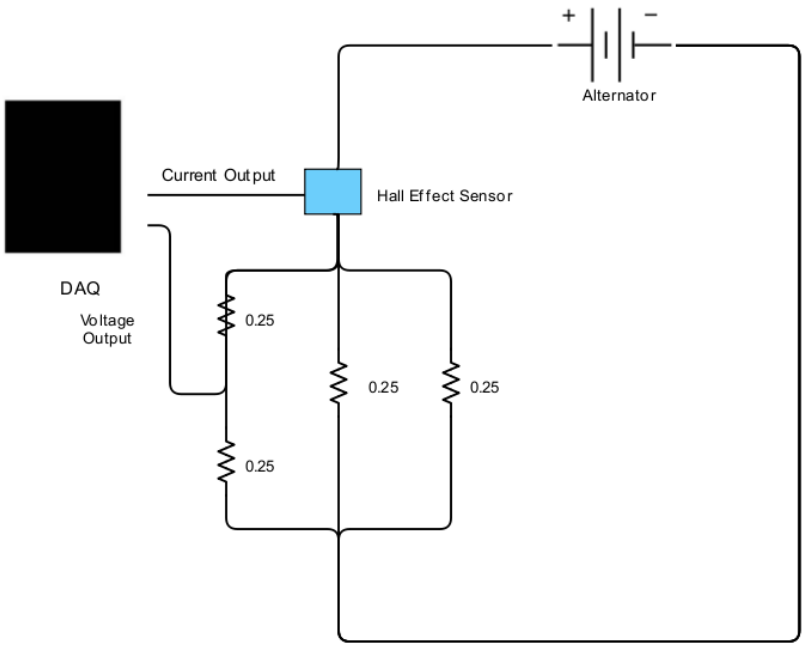

Fig. 18. Current and voltage sensor schematic

3.8 Alternator Retrofitting and Disassembly

Once the test rig had been assembled, the team must determine how to integrate the optimized 4 and 8-pole salient rotors into an alternator assembly. As shown in Fig. 19 below, the alternators disassemble into individual parts to use or change, and the team has dismantled them in an on-campus lab. The team cannot feasibly construct its own aluminum housing, stator, and other components of an alternator; however, the team can purchase parts of a dismantled alternator from a standard auto parts dealer after receiving the necessary quality checks. The main difference between existing alternators and the team's modified alternator will be the rotor; a 4 or 8-pole salient rotor will take the place of a default Lundell rotor. In current alternators, the rotor shaft serves to electromagnetically induce a current in the stator windings by rotating the electromagnet in the rotor within the stator [14]. This rotation is achieved by attaching the rotor shaft to a pulley system, which is in turn connected to the crankshaft [36].

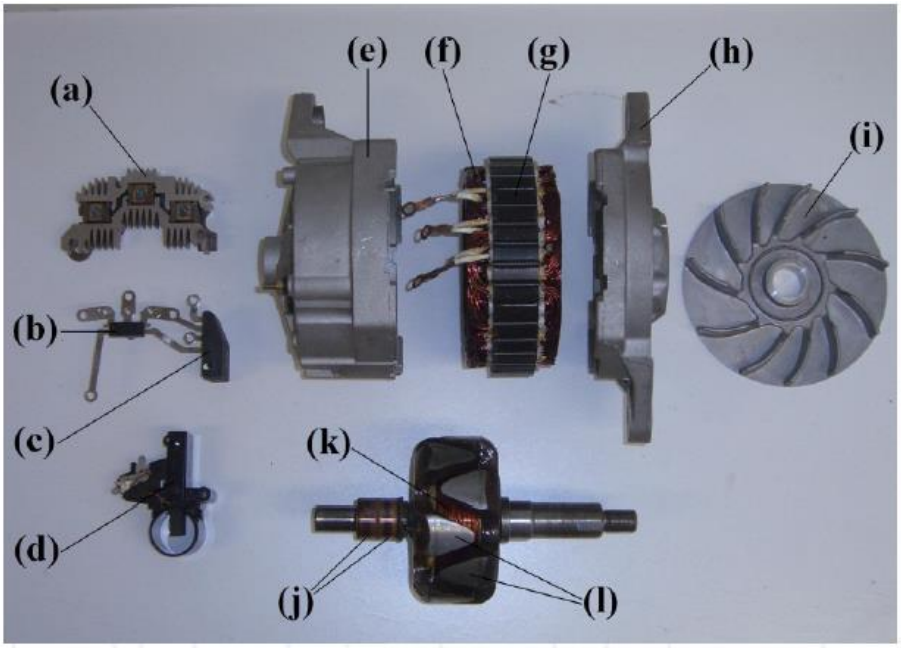

Fig. 19. Dismantled alternator: 6 diode full-bridge power rectifier, (b) excitation rectifier, (c) regulator, (d) brush assembly, (e) aluminum rear housing, (f) stator winding, (g) stator laminated core, (h) aluminum front housing, (i) aluminum fan, (j) slip rings, (k) excitation winding, and (l) claw-shaped pole pieces. [16]

During Maxwell simulations, the team will optimize geometric features of the 4 and 8-pole salient rotors to test the effect on power output and torque output. The Lundell alternator will also be tested in Maxwell as a basis for comparison. The salient rotors were constrained to fit within an existing alternator housing, as the team will not design and fabricate its own housing. There will be a control alternator that will have had no changes in order to establish a baseline to which all measurements of power output and braking torque can be compared. As stated before, the control alternator will house the control rotor, a Lundell rotor. As discussed in Sections 3.7 and 3.8, a custom test rig and sensor setup was used to determine the power output and braking torque of the Lundell rotor. The recommendations that the team makes regarding the 4-pole and

8-pole salient rotors are targeted for the implementation within the alternator housing used in this study. Different alternator housings would lead to different constraints on the dimensions of the 4 and 8-pole rotors, leading to different rotors and different final recommendations. During this testing, output torque would be measured using a torque/speed transducer, and power output will be measured using the voltmeter with a serial output. Afterwards, the two recommended 4 and 8-pole salient rotors would be reassembled into the housing of the alternator. These different alternator assemblies would then be tested as a whole to determine which rotor shape can lead to an increase in power output and braking torque. Also, the experimental results would be used to validate the Maxwell simulation results and provide a better estimate of the efficiency of the alternator as a whole.

3.9 Rotor Fabrication

As discussed in Section 2.5, the recommended rotor core will be fabricated from high purity ARMCO iron ingots due to its ideal magnetic properties. ARMCO iron ingots have a minimum purity of 99.85% and after melting, they undergo vacuum degassing which produces a homogenous structure after solidification. ARMCO Pure Iron has also been used in the production of magnets, such as pole cores and armatures, strengthening their selection as a core material for the team's application. The team machined the rotor cores from the ARMCO Pure Iron ingots rather than use any form of processing due to the possibility of compromising the magnetic properties of the material. The magnetic properties of ARMCO Pure Iron can be compromised if the material is subjected to cold processing, but since the team will only concern itself with machining the rotor cores from the ingots, the team will not need to worry about the

consequences of cold processing. Also, the magnetic properties of the material can be compromised at elevated temperatures if the Curie Temperature is exceeded, which can cause the dipoles of the material to misalign.

3.10 Magnet Wire and Rotor Winding

Since alternators experience temperatures of up to 200 °C, the team recommends the use of 18 AWG solid core copper wire with a polyester-imide coating [16]. This magnet wire falls under the 180 °C thermal grade, meaning that it will degrade after approximately 5,000 hours at 200 °C. Although the test rig setup will not reach the same temperatures as an alternator in the hood of a car, the research team will need to closely monitor the temperature of the magnet wire material. Information about how the temperature will be monitored can be found in Section 3.8.

One of the greatest lurking variables that will serve as a constant obstacle to testing the efficacy of the different rotor designs will be how the electromagnet coils are created. If coiling patterns differ from test group to test group, the results will be skewed. The coil pattern of the electromagnets is directly related to how strong an electric field is generated onto the coils [37]. For example, a more densely packed electromagnet will be able to create larger magnetic fields, resulting in greater changes in magnetic flux, and therefore leading to an increase in electrical power [12]. In an attempt to reduce the effect of differences in magnet wire coiling pattern, we recommend that only one person should be responsible for creating all electromagnet coils, since coil patterns may vary from person to person.

Once the rotor core is machined, the magnet wire can be wound around the rotor poles. To accomplish this, a single person should carefully hand-wind the rotor such

that there is no spacing between each loop of the coil. The direction of the winding needs to be alternated between clockwise and counterclockwise in order to achieve alternating magnetization of the poles, as seen in Fig. 20.

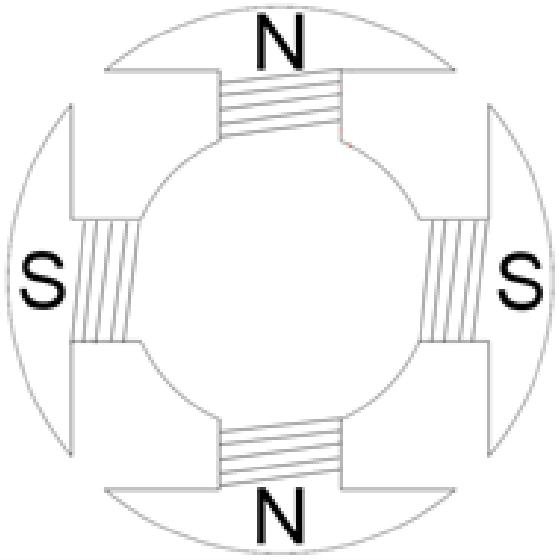

Fig. 20. Alternating poles of 4-pole salient rotor

3.11 Conclusion

Overall, the research team will be focusing on optimizing the electrical output and braking torque from an alternator through the manipulation of two independent variables: magnet wire material and rotor shape. From testing the two different independent variables of magnet wire material and rotor shape, the group hopes to come to a conclusion regarding which combination of the two variables will lead to an increase in alternator power efficiency and braking torque efficiency. In Chapter 4, the team will analyze the data from the Maxwell simulations so that a final recommendation can be made for the implementation of a 4-pole and 8-pole rotors in an alternator-based regenerative braking device for drive shaft application.

Chapter 4: Discussion of Results

4.1 Introduction

In this section, the team will discuss the results from the Maxwell simulations and the test rig experiments. The steps in which the DOE methodology were taken to optimize the 4 and 8-pole rotor geometry will be explained. At the end of the section, the team will recommend a strategy for optimizing the rotor geometry of the 4-pole and 8-pole rotors so that maximum braking torque can be achieved using the alternator model used in the team's research.

4.2 Results from Maxwell Simulations

4.2.1 4-Pole Rotor

After running the 9 preliminary rotors with the geometries detailed in Section 3.4 in Maxwell, the induced current and voltage values at each tested RPM were then used to calculate the produced electrical power at each RPM. Under the assumption that each rotor is perfectly efficient, the maximum braking torque was determined from the maximum electrical power produced. This relationship can be found in Equation 2. Across the range of angular velocity range being tested, the electrical power dropped linearly from its maximum at the highest angular velocity, 2300 RPM, down to its minimum tested RPM at 100 RPM. As expected the maximum electrical power produced occurred during the maximum rotation speed, because this is directly translated to the greatest rate of change of magnetic flux. Even though electrical power would decrease at lower angular velocities, the estimated braking torque would remain approximately the same, considering the relationship shown in Equation 2. Electrical power produced would decrease at the same rate as the angular velocity, so braking torque would be largely unaffected. Therefore, average braking torque was taken as the

variable that would determine the next set of rotors that would be tested. The average braking torque results from the preliminary Maxwell experiment can be seen in Fig. 21.

$$\tau = \frac{P}{\omega}$$

Equation 2. Relationship between braking torque (τ), electrical power production (P), and drive shaft angular velocity (ω) for the alternator-based regenerative braking system

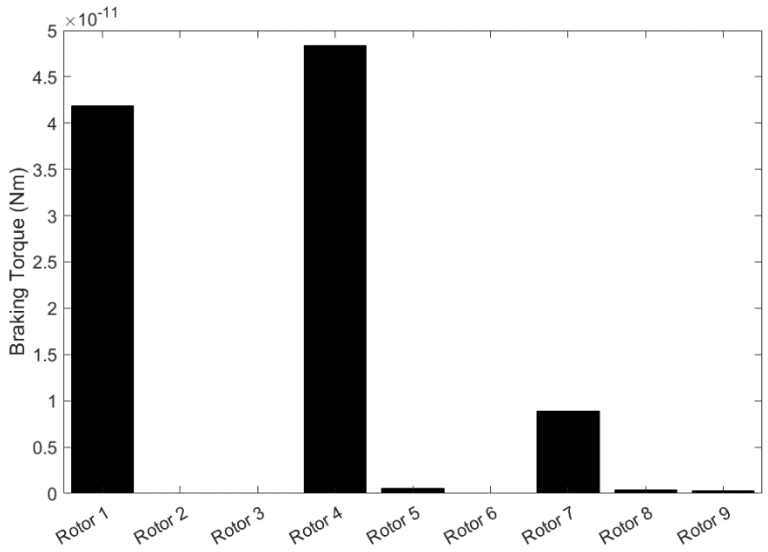

Fig. 21. Preliminary 4-pole rotor results. Each group of three rotors represent a set of rotors with similar P_h but different P_t. Every third rotor represents a rotor with similar P_t, but different P_h.

As seen in Fig. 21, there are several peaks of average braking torque, at rotors 1, 4, and 7. These three rotors all had the same P_t and different P_h. A closer look shows that lower P_t leads to an increase in braking torque. One explanation for this trend is that a smaller P_t leads to a more concentrated magnetic flux. Also, there was less interference between the windings of the poles, leading to an increase in the number of

windings. An increase in the number of windings would also increase the magnetic flux magnitude.

From these results, several more Maxwell simulations were run while maintaining the same P_t but introducing more rotors between the lower and upper bounds of P_h, 23.385 mm and 44.2 mm, which were defined by rotors 1 and 7 of the preliminary simulations of the 4-pole rotors. These simulations helped determine if there was an optimal P_h that would lead to the greatest average braking torque. It was predicted that the greatest P_h would lead to the greatest average braking torque; the greatest P_h leads to the greatest number of windings, therefore producing the greatest magnetic flux and braking torque. However, the effect of the rotor heads is not fully understood. There could be adverse effects, such as the shielding of magnetic flux, that negatively affect the results. Field lines would travel from the solenoid that is created from the windings about the pole arm. However, these field lines would also be directed to the pole heads, rather than the stator, leading to a decrease in the amount of magnetic flux captured by the stator. This redirection of field lines can be seen in Fig. 22.

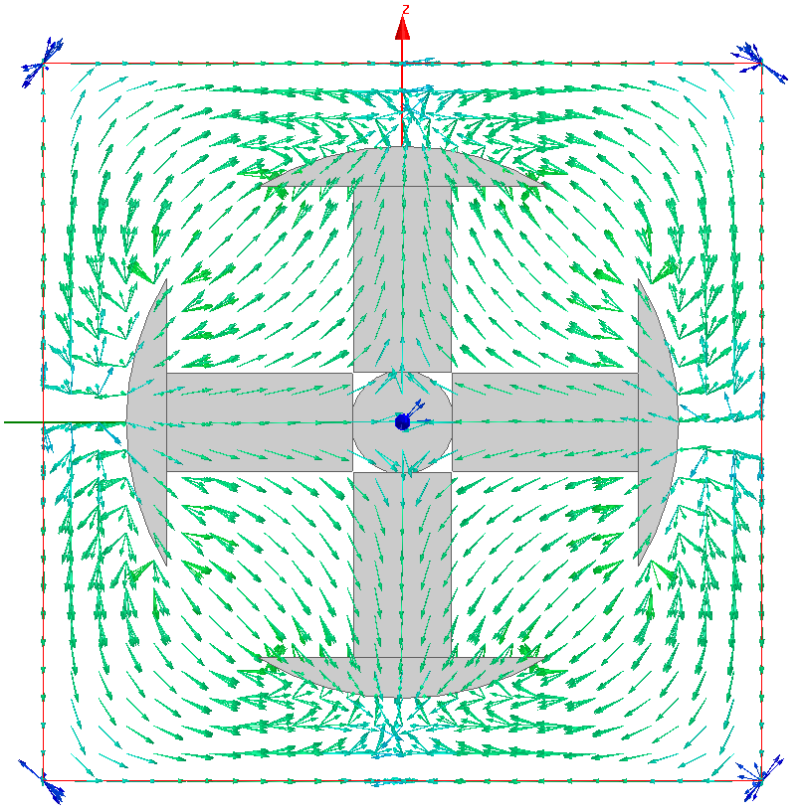

Fig. 22. Sample rotor demonstrating the redirection of magnetic field lines towards the pole heads.

The rotor heads could not be removed because they would ensure that the rotor windings remain in place on the rotor. Figures 21-23 shows the magnetic flux diagrams of Rotors 1, 4, and 7, respectively. As seen in Figures 21-23, the heads play an important role in the magnetic flux distribution of each rotor. Rotor 1 has a more continuous distribution of magnetic flux and since induced voltage is dependent on rate of change of flux, Rotor 1 will not have induced as large of a voltage as Rotor 4.

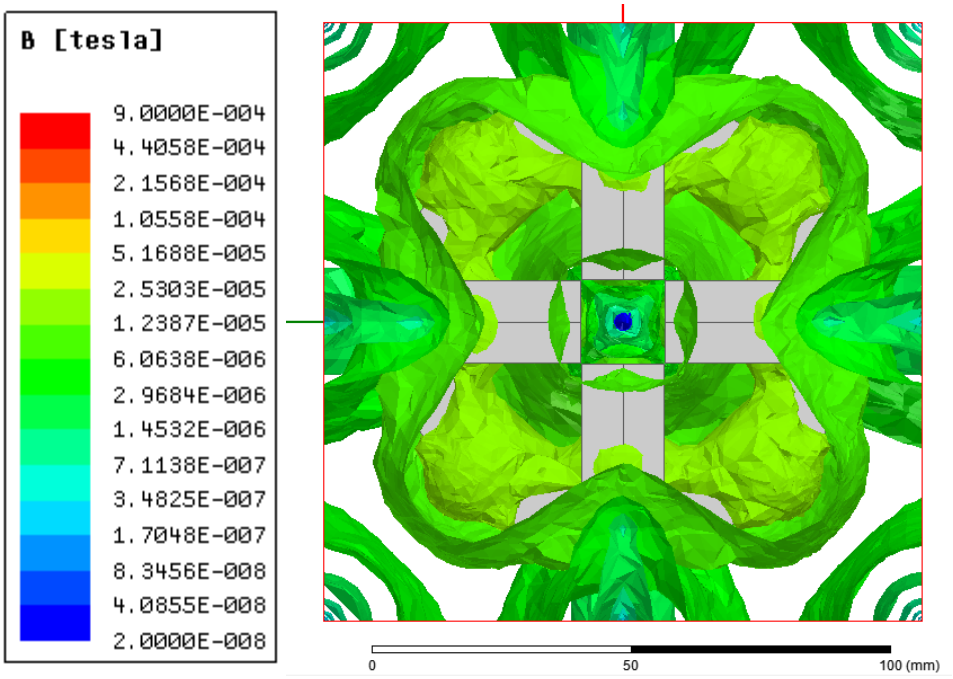

Fig. 23. Rotor 1 of 4-pole preliminary simulations

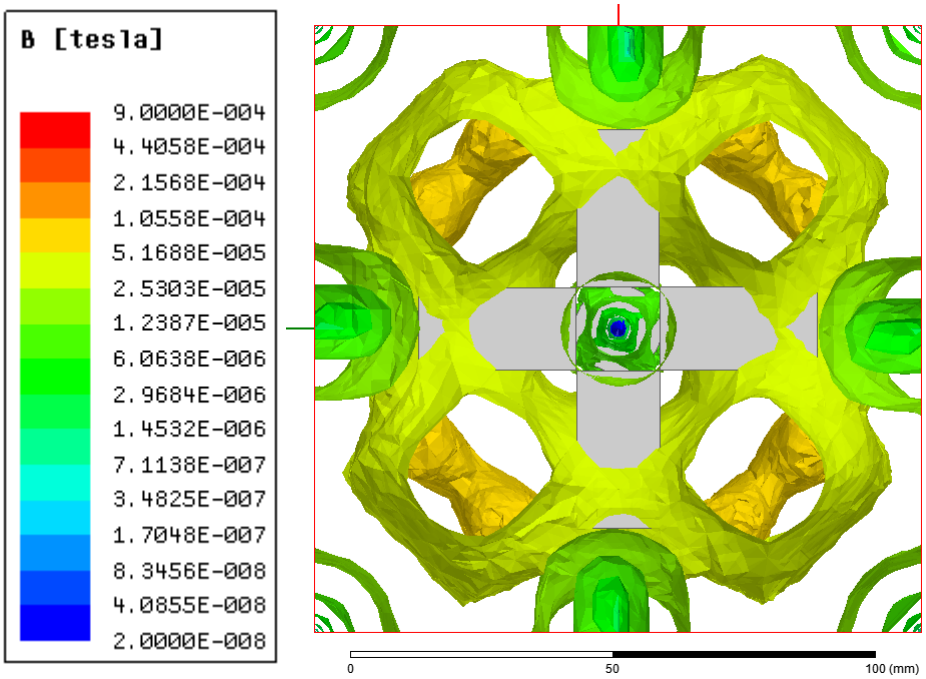

Fig. 24. Rotor 4 of 4-pole preliminary simulations

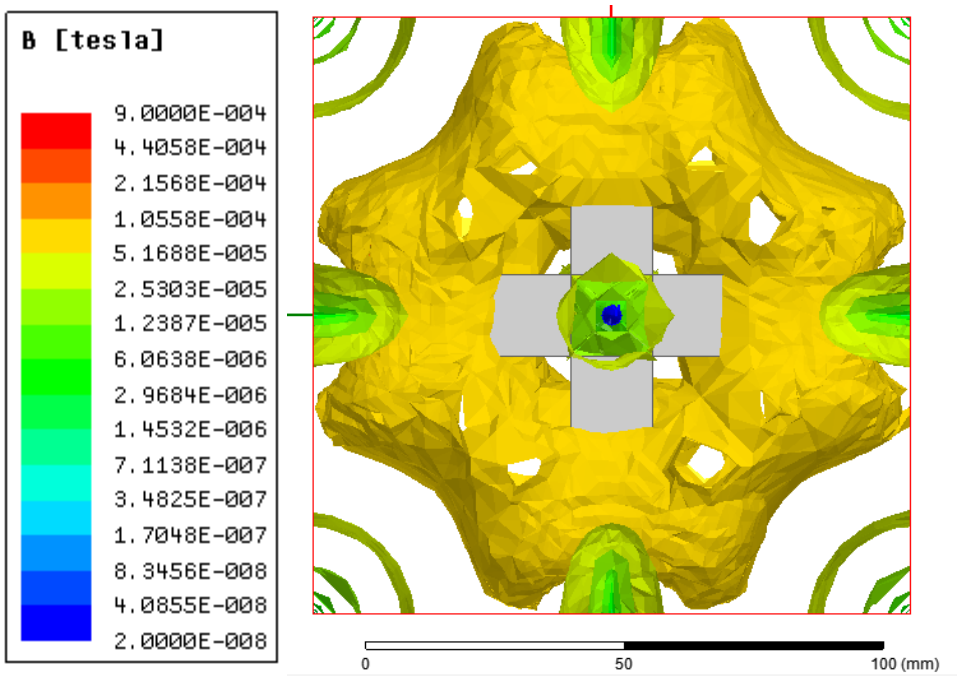

Fig. 25. Rotor 7 of 4-pole preliminary simulations

The results from the Maxwell simulations with rotors of equal P_t are shown in Fig. 26. The general trend of increasing P_h while maintaining P_t is correlated with an increase of the maximum braking torque. There are a few explanations for this trend. First, with an increase in P_h, there is an increase in the number of windings. With more windings, the salient rotor is able to produce a greater magnetic flux. A smaller pole head is correlated with an increase in magnetic flux that is captured by the stator. The rotor head acts as a region where magnetic flux can be blocked. Field lines converge on the rotor heads, and the larger the rotor head, the greater the number of field lines that converge onto the rotor heads. An increase in the number of field lines also correlates with an increase in the amount of magnetic flux. Therefore, a greater concentration of magnetic flux is captured by the larger pole heads, as opposed to the stator. In an ideal case, the pole heads could be removed, to increase the amount of

magnetic flux captured by the stator, however, the pole heads are required to keep the windings in their position when the rotor is rotating.

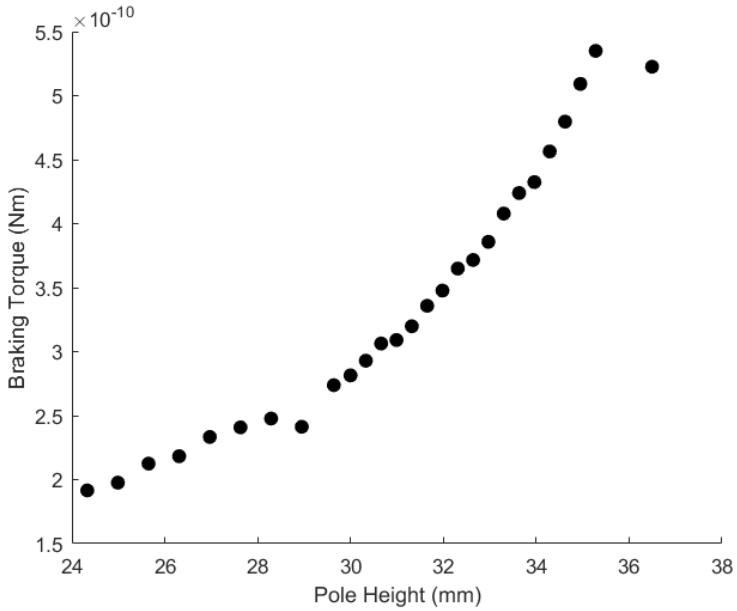

Fig. 26. Average braking torque with P_t=5mm

4.2.2 8-Pole Rotor Results

A total of three different designs of the 9 rotor iterations were developed to determine the most optimal configuration. Similar to the 4-pole analysis, the most optimal design would then produce the largest braking torque and reveal trends in how rotor dimensions affect output current and voltage.

The first design made no changes to the dimensions presented in Table 4 for the 9 different rotor iterations. Instead, it was found that due to the increased number of poles present in the constrained area, maintaining an exterior diameter of 90 mm for each of the heads resulted in interference. To counteract this physical limitation, the heads were truncated at the point of interference, leaving a 0.10 mm gap between neighboring pole heads. The gap is present to allow the CAD software to resolve two

separate faces and parts. A sample 8-pole rotor with truncated heads can be found in Fig. 27.

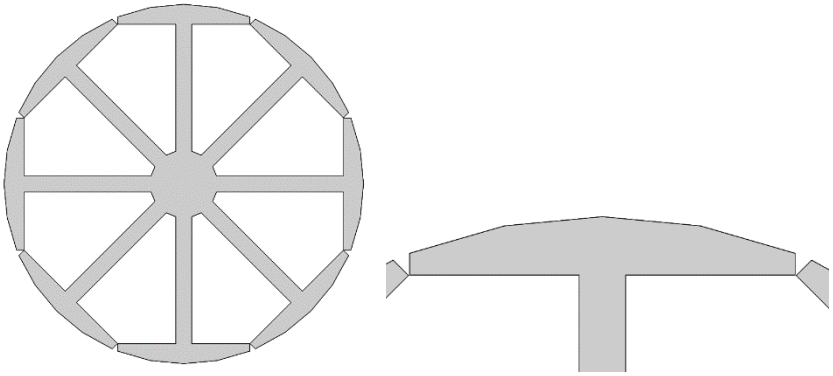

Fig. 27. Rotor 1 truncated heads and detailed view

The simulated maximum braking torques found for this first round of analysis are summarized in Fig. 28. The average braking torques are calculated in the same manner as for the 4-pole analysis. The rotor iterations with the largest generated braking torques were 1, 5, and 6. However, there was no conceivable trend found within these particular rotor iterations across any of the rotor dimensions. A trend would help in further narrowing down the most optimal rotor configurations. Rotors 7-9 demonstrate a decreasing sub-trend corresponding to a decrease in pole height with a constant pole thickness. However, this relation is unique as it is not replicated in other rotors that share the same pole thickness.

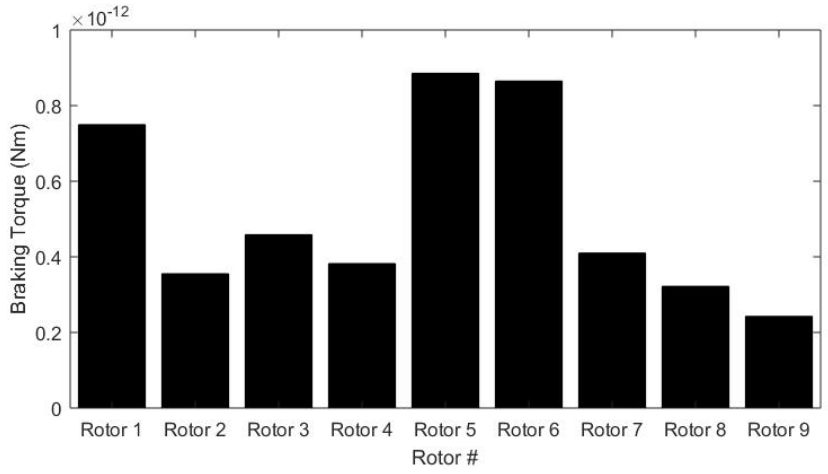

Fig. 28. Truncated head braking torques

Instead, the truncated head shape likely resulted in skewed magnetic field lines. Truncating the heads introduced a flat face at the tips of each pole head. Since magnetic field lines enter and leave ferromagnetic materials perpendicular to the surface, part of the magnetic field is concentrated between these flat faces. The field generated does not extend beyond the rotor diameter to the point in space where the stator exists nearly as much as it would with different head shapes. As mentioned prior, this concern leads to a decrease in the magnetic flux captured by the stator. The magnetic field line behavior is exhibited in Fig. 29.

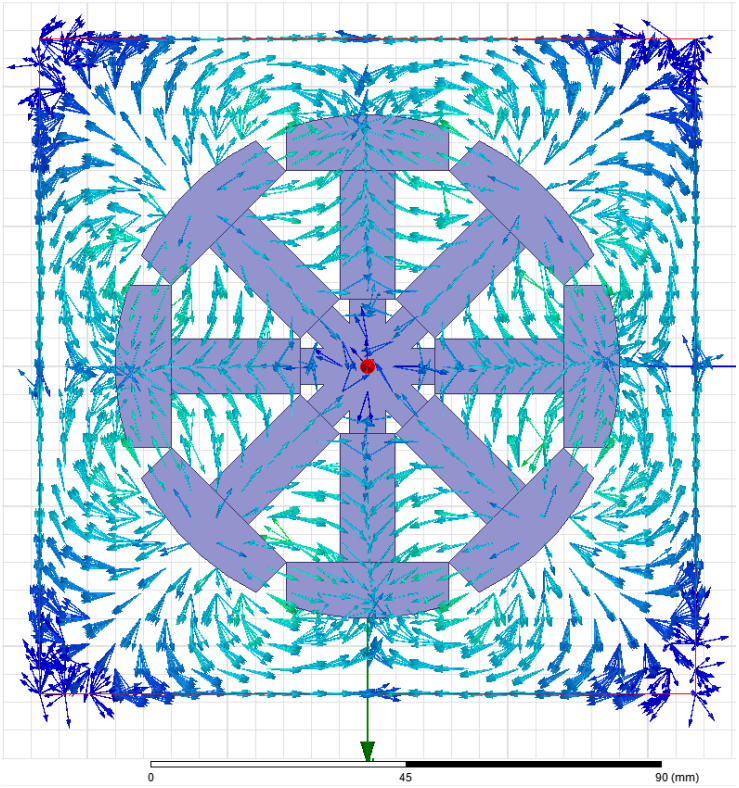

Fig. 29. Planar magnetic field lines for rotor 9 with truncated heads

To remove this confounding influence of the truncated rotor heads from the analysis and isolate the poles, a new design was developed where the rotor iterations lacked any pole ends and thus heads. As seen in Fig. 30, the pole head is left off from the rotor core design while all remaining dimensions were kept the same. This design is not feasible in a real-life application but merely used here for analysis.

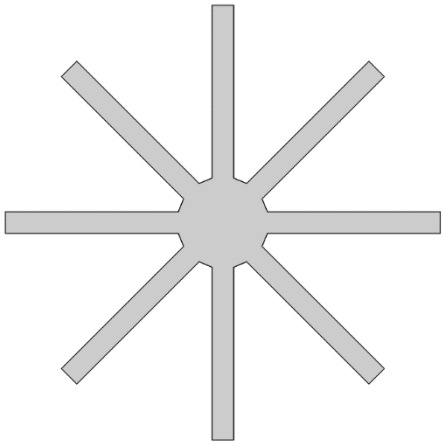

Fig. 30. Headless rotor 1 configuration

The braking torque generated by these new models demonstrated a much clearer trend, as shown in Fig. 31. Here, the braking torque reveals an internal trend within each grouping of 3 rotors as well as an overarching trend across each group. This internal trend is similar to the outlying trend seen in rotors 7-9 of the first design analysis. Recalling the numbering scheme of the rotor iterations, the pole thickness is held constant for 3 rotor iterations at a time and increased in value for each group. Within each pole thickness value, the pole height is varied in a descending pattern. This means the first rotor iteration has the thinnest and tallest pole while the last iteration has the thickest and shortest.

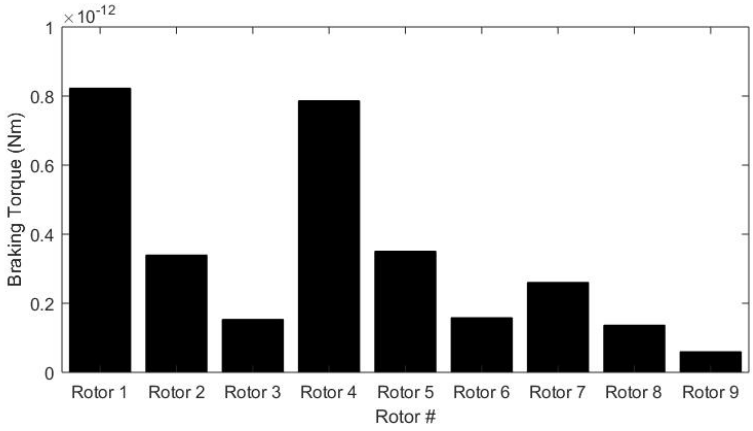

Fig. 31. Headless rotor braking torques

These combinations of dimensions produce unique numbers of total windings, which directly correspond to the braking torque magnitudes. The increase in winding number is a product of the thinner pole thickness and taller pole height: more layers of windings and stacks of windings fit within the remaining space. Furthermore, the second design analysis reveals that the truncated head shape indeed had an influence on the magnetic output and thus braking torque magnitude.

To better test this influence and confirm the observed trend, the last design reintroduced pole heads with varying curvatures instead of fixed outer radii. Rather than constraining the arc radius of each pole head to the 90 mm outer diameter, the new designs allow each arc to match the truncated cord length while remaining tangent to the outer diameter. A depiction of a reshaped 8-pole rotor can be found in Fig. 32. The same 0.10 mm gap is left in between pole heads to help differentiate surfaces.

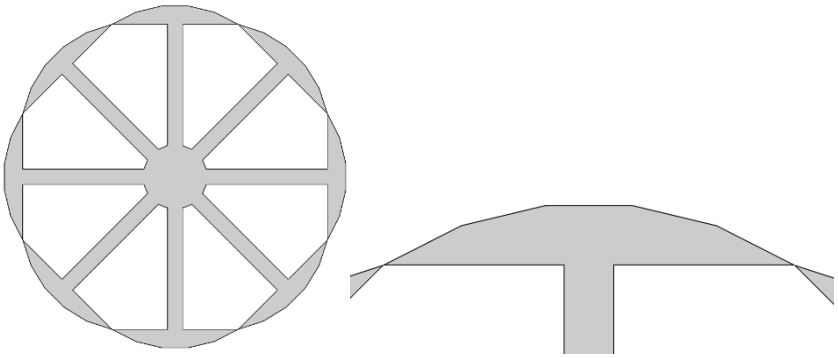

Fig. 32. Reshaped rotor 1 heads and detailed view

Since these rotors no longer share the same flat faces the truncated rotors do, the magnetic field lines behave differently. They extend further into the surrounding space and allow the stator to capture more of the magnetic flux than before. The magnetic field line behavior of a reshaped 8-pole rotor can be found in Fig. 33.

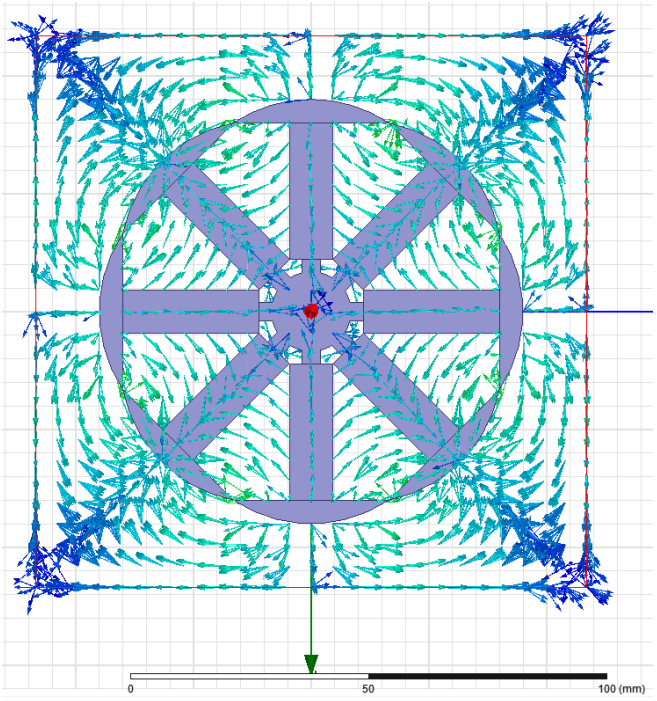

Fig. 33. Planar magnetic field lines for rotor 9 with reshaped heads

The braking torques generated from the resulting output current and voltage match the trend exhibited for the second design and can be seen in Fig. 34. The magnitudes of the largest braking torque increase by a factor of approximately 4 and show a heavier influence on the rotors with thinner poles (earlier rotor iteration numbers). However, this may be due to the length of the extruded pole. The designs lacking pole ends did not extrude the individual pole heights to the same outer diameter of 90 mm. Instead, they were merely removed at the shared face with the pole body. As a result, the magnetic field strength varied and was weaker at the location of the stator, which remained the same across each simulation and was where data was collected. This unintended consequence was then noted for future simulations, as the preliminary headless design was to only serve as a control group for basic comparative analysis.

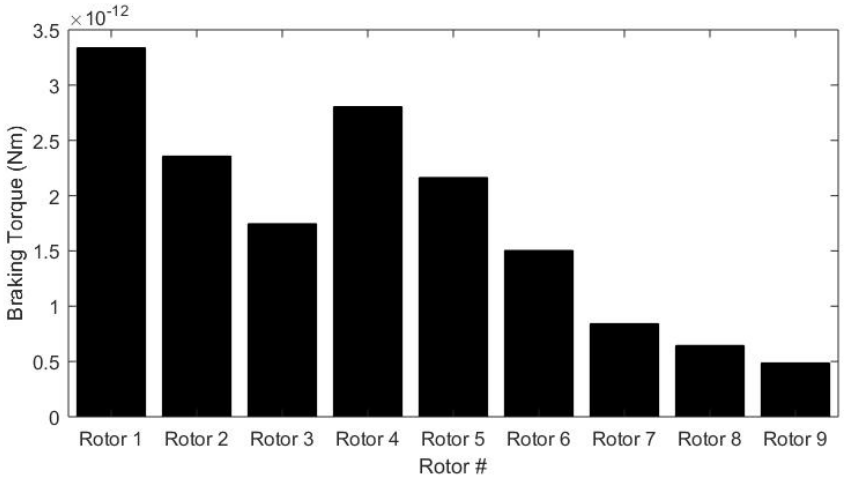

Fig. 34. Reshaped 8-pole rotor braking torques

Once again, the best performing rotor iterations are those that possess a larger number of windings. Rotors 1, 2, and 3 respectively fit 102, 93, and 96 windings around each of the 8 poles. This is significantly larger than the 54 windings fit around the poles

of rotor 9. Note that the higher number rotors (7-9) performed the worst since only 2 layers of winding, shown in Table 5, could fit around the thicker poles. A larger number of windings results in a stronger generated magnetic field within the coil. The increase in strength then magnetizes the ferromagnetic core further and leads to a larger magnitude of magnetic flux seen at the stator.

Further analysis needs to be conducted with constant, thin pole thickness to observe the influence of the head size and determine the relationship of pole height and thickness to winding number. This can be done by holding variables constant across the rotor iterations and testing individual factors. Also, new headless rotors will be tested where the pole heights are extruded to the maximum 90 mm outer diameter. This will present a more comparable control group to judge the effects of the pole ends on magnetization and flux strength.

Chapter 5: Conclusion

After finishing the simulations for the 4-pole and 8-pole salient rotor, the team was able finalize several recommendations for electromagnetic rotor geometry to be used in a regenerative braking system on an automobile's drive shaft. Based on existing literature, the team recommends the use of high purity iron for the ferrous core material because of its material properties. Iron allows the generated magnetic field to react quickly to a user's input, while maximizing magnetic field output. Also, from an analysis of tolerances, the team recommends wire EDM as the manufacturing method for the rotors to minimize adverse effects from other machining methods and to minimize tolerances.

The Maxwell simulations have also resulted in several important insights regarding rotor geometry and type. It was shown that by maximizing the pole height and minimizing the pole thickness of the 4-pole rotors, the average braking torque was maximized. This result can be explained by an increase in the number of windings, an increase in the concentration of magnetic flux, and a decrease in the redirection of magnetic field lines to the pole head. The 8-pole simulation results also exhibited a similar trend. The best rotor design also implements a smaller pole thickness and taller pole height to facilitate greater winding packaging. The limiting factors would then be machining tolerance and structural rigidity of the rotor construction. Further simulations will need to be conducted in order to confirm the influence of the pole head on the magnetic field generation.

From these anticipated results, new areas of future research can benefit. For example, although the research team was unable to implement the recommended 4-

pole and 8-pole rotors into the alternator, these recommendations can be used to guide the research and future works of other researchers. Future work could also include implementing the recommended rotors onto a vehicle. Afterwards, researchers can explore the feasibility of the design and how it fares in different driving conditions. In conclusion, even though the research team was unable to fully carry out the overall intent of implementing the team's design onto a vehicle, the team has provided the instructions for future research to integrate the team's system into an automobile. The research conducted by Team DRIVE will then provide an advancement of the current state of automotive hybrid technology. Such an expansion of the field will have a positive effect on the consumer and environmental impact of automobiles.

Bibliography

[1] E. A. Nanaki and C. J. Koroneos, “Comparative economic and environmental analysis of conventional, hybrid and electric vehicles - the case study of Greece,” *J. Clean. Prod.*, vol. 53, pp. 261–266, 2013.

[2] “CO2 emissions from transport (% of total fuel combustion) | Data.” [Online]. Available: https://data.worldbank.org/indicator/EN.CO2.TRAN.ZS. [Accessed: 25-Apr-2018].

[3] D. L. Greene, K. G. Duleep, and W. McManus, “Future Potential of Hybrid and Diesel Powertrains in the U.S. Light-Duty Vehicle Market,” Oak Ridge National Laboratory, Aug. 2004.

[4] H. Bathelt, “Motor-vehicle drive-shaft assembly,” 4,232,756, 11-Nov-1980.

[5] Ford, “2018 F-150 XL,” *Explore 2018 Ford F-150*. [Online]. Available: https://www.ford.com/trucks/f150/models/f150-xl/.

[6] S. Shea, “54.5 MPG and Beyond: Materials Lighten the Load for Fuel Economy,” *Department of Energy*. [Online]. Available: https://www.energy.gov/articles/545-mpg-and-beyond-materials-lighten-load-fuel-economy.

[7] K. T. Chau, Ming Cheng, C. C. Chan, “Performance Analysis of 8/6-Pole Doubly Salient Permanent Magnet Motor,” *Electr. Mach. Power Syst.*, vol. 27, no. 10, pp. 1055–1067, Sep. 1999.

[8] M. Grayen, “The Difference Between A Transaxle And A Transmission,” *CARiD.com*. [Online]. Available: https://www.carid.com/articles/transaxle-vs-transmission.html. [Accessed: 03-Apr-2017].

[9] G. Magliano, “US - Light Vehicle Outlook,” presented at the Detroit Association for Business Economics’ Automotive and Economic Outlook Luncheon, Detroit, MI, Jan-2012.

[10] T. Muro, “Comparison of the traffic performance of a two-axle four wheel drive (4WD), rear wheel drive (RWD), and front wheel drive (FWD) vehicle on loose sandy sloped terrain,” *J. Terramechanics*, vol. 34, no. 1, pp. 37–55, 1997.

[11] S. J. Hallowell and L. R. Ray, “All-Wheel driving using independent torque control of each wheel,” presented at the American Control Conference, Denver, 2003, pp. 2590–2595.

[12] R. D. Knight, *Physics for Scientists and Engineers*, 3rd ed. Pearson, 2013.

[13] M. Riaz, “ALTERNATOR.” [Online]. Available: http://people.ece.umn.edu/users/riaz/animations/alternator.html. [Accessed: 05-Apr-2017].

[14] M. Bradfield, “Improving alternator efficiency measurably reduces fuel costs,” Remy Inc., 2008.

[15] D. M. Whaley, W. L. Soong, and N. Ertugrul, “Exctracting more power from the lundell car alternator,” presented at the Australasian Universities Power Engineering Conference, Brisbane, 2004.

[16] R. Ivankovic, J. Cros, M. T. Kakhi, C. A. Martins, and P. Viarouge, “Power Electronic Solutions to Improve the Performance of Lundell Automotive Alternators.” InTech, 2012.

[17] M. Comanescu, A. Keyhani, and M. Dai, “Design and Analysis of 42-V Permanent-Magnet Generator for Automotive Applications,” *IEEE Transactions on Energy Conversion*, vol. 18, no. 1, pp. 107–112, Mar. 2003.
[18] V. Pricop, G. Scutagu, and E. Helerea, “Magnetic Materials for Accelerator Electromagnets,” *Ser. Eng. Sci.*, vol. 6, no. 55, 2013.
[19] W. Yin, “Dielectric properties of an improved magnet wire for inverter-fed motors,” *IEEE Electr. Insul. Mag.*, vol. 13, no. 4, pp. 17–23, Jul. 1997.
[20] R. Beeckman, “NEMA Magnet Wire Thermal Class Ratings.” [Online]. Available: https://www.superioressex.com/uploadedFiles/News/White_Papers/emcwa-nema_magnet-thermal-class-ratings.pdf. [Accessed: 05-Apr-2017].
[21] A. Pilat, “FEMLab software applied to active magnetic bearing analysis,” *Int. J. Appl. Math. Comput. Sci.*, vol. 14, no. 4, pp. 497–501, 2004.
[22] J. G. Zhu, “Synchronous Machines,” *Electrical Energy Technology*, 2008. [Online]. Available: http://services.eng.uts.edu.au/cempe/subjects_JGZ/eet/eet_ch6.pdf. [Accessed: 06-Nov-2016].
[23] L. Simplified, “Introduction, Constructional Details ,Types of Rotor ,Exciter of Three Phase Synchronous Generator.” [Online]. Available: https://www.kullabs.com/classes/subjects/units/lessons/notes/note-detail/2796. [Accessed: 18-Aug-2017].
[24] A. Reddy, “Principle & working of Synchronous generator or Alternator,” *Electical Engineering Info*. [Online]. Available: http://www.electricalengineeringinfo.com/2014/08/principle-and-working-of-synchronous-generator-alternator.html.
[25] K. Daware, “Salient pole rotor vs. non-salient pole rotor.” .
[26] H. Hamada, “Alternator having Lundell type rotor,” US7592735 B2, 22-Sep-2009.
[27] I. Boldea, *Variable Speed Generators*. CRC Press, 2005.
[28] E. Abdo, *Power Equipment Engine Technology*. Clifton Park: Delmar, Cengage Learning, 2011.
[29] M. Bradfield, “Thermal Design Challenges in Automotive Alternator Power Electronics | Electronics Cooling,” *Electronics Cooling*, 01-May-2002. [Online]. Available: https://www.electronics-cooling.com/2002/05/thermal-design-challenges-in-automotive-alternator-power-electronics/#. [Accessed: 01-Apr-2018].
[30] M. K. Yoong *et al.*, “Studies of regenerative braking in electric vehicle,” in *IEEE Conference on Sustainable Utilization and Development in Engineering and Technology*.
[31] M. J. Melfi, “Optimum pole configuration of AC induction motors used on adjustable frequency power supplies,” presented at the Petroleum and Chemical Industry Conference, Denver, 1995.
[32] D. E. Breese, K. L. Stevens, and C. C. Cheney, *Driveshaft assembly having a noise reduction structure*. Google Patents, 2001.
[33] Northwest Wire EDM, “Wire EDM Frequently Asked Questions.” [Online]. Available: http://www.northwestwireedm.com/wire_edm_faqs.php. [Accessed: 01-Apr-2018].

[34] Proto Labs, “CNC Milling Machining Design Guidelines,” *Proto Lab Services*. [Online]. Available: https://www.protolabs.com/services/cnc-machining/cnc-milling/design-guidelines/. [Accessed: 01-Apr-2018].
[35] B. Olding and N. Eagle, “Using an Alternator in Renewable Energy Projects,” *Nepal Ghatta Project*. [Online]. Available: http://alumni.media.mit.edu/~nathan/nepal/ghatta/alternator.html. [Accessed: 01-Apr-2018].
[36] A. Michelotti, A. Paza, A. Maurici, and C. Foppa, “Future Trends in the Conceptual Design Alternator Pulleys,” *21st SAE Bras. Int. Congr. Exhib.*, 2012.
[37] S. E. Gay, “Contactless magnetic brake for automotive applications,” Doctoral Dissertation, Texas A&M University, 2005.